HHS Public Access

Author manuscript

Neuropharmacology. Author manuscript; available in PMC 2022 December 01.

Published in final edited form as:

Neuropharmacology. 2022 December 01; 220: 109271. doi:10.1016/j.neuropharm.2022.109271.

The $Ca_V1.2$ G406R mutation decreases synaptic inhibition and alters L-type Ca^{2+} channel-dependent LTP at hippocampal synapses in a mouse model of Timothy Syndrome

Jennifer L. Sanderson[a], **Ronald K. Freund**[a], **Anna M. Castano**[a], **Timothy A. Benke**[a,b], **Mark L. Dell'Acqua**[a,*]

[a]Department of Pharmacology, University of Colorado School of Medicine, Anschutz Medical Campus, 12800 E. 19th Ave, Mail Stop 8303, Aurora, CO, 80045, USA

[b]Departments of Pediatrics, Neurology, and Otolaryngology, University of Colorado School of Medicine, Anschutz Medical Campus, 12800 E. 19th Ave, Mail Stop 8303, Aurora, CO, 80045, USA

Abstract

Genetic alterations in autism spectrum disorders (ASD) frequently disrupt balance between synaptic excitation and inhibition and alter plasticity in the hippocampal CA1 region. Individuals with Timothy Syndrome (TS), a genetic disorder caused by $Ca_V1.2$ L-type Ca^{2+} channel (LTCC) gain-of function mutations, such as G406R, exhibit social deficits, repetitive behaviors, and cognitive impairments characteristic of ASD that are phenocopied in TS2-neo mice expressing G406R. Here, we characterized hippocampal CA1 synaptic function in male TS2-neo mice and found basal excitatory transmission was slightly increased and inhibitory transmission strongly decreased. We also found distinct impacts on two LTCC-dependent forms of long-term potentiation (LTP) synaptic plasticity that were not readily consistent with LTCC gain-of-function. LTP induced by high-frequency stimulation (HFS) was strongly impaired in TS2-neo mice, suggesting decreased LTCC function. Yet, $Ca_V1.2$ expression, basal phosphorylation, and current density were similar for WT and TS2-neo. However, this HFS-LTP also required $GABA_A$ receptor activity, and thus may be impaired in TS2-neo due to decreased inhibitory transmission. In contrast, LTP induced in WT mice by prolonged theta-train (PTT) stimulation in the presence of a β-adrenergic receptor agonist to increase $Ca_V1.2$ phosphorylation was partially induced

*Corresponding author. mark.dellacqua@cuanschutz.edu (M.L. Dell'Acqua).

Author contributions

Conceptualization, M.L.D., J.L.S., R.K.F., T.A.B, and A.M.C.; Methodology, J.L.S., R.K.F., A.M.C., and T.A.B.; Formal Analysis and Investigation: M.L.D., J.L.S., R.K.F., T.A.B, and A.M.C.; Resources, M.L.D. and T.A.B; Writing-Original Draft, M.L.D; Writing-Review & Editing, M.L.D., J.L.S., R.K.F., T.A.B, and A.M.C.; Supervision, M.L.D. and T.A.B. Funding Acquisition, M.L.D. and T.A.B.

Declaration of competing interest

The authors declare no competing interests.

Appendix A. Supplementary data

Supplementary data to this article can be found online at https://doi.org/10.1016/j.neuropharm.2022.109271.

Chemical compounds studied in this article:

Nimodipine

Isoproterenol

Picrotoxin

in TS2-neo mice by PTT stimulation alone, consistent with increased LTCC function. Overall, our findings provide insights regarding how altered $Ca_V1.2$ channel function disrupts basal transmission and plasticity that could be relevant for neuro-behavioral alterations in ASD.

This article is part of the Special Issue on 'L-type calcium channel mechanisms in neuropsychiatric disorders'.

Keywords

L-type calcium channel; Timothy syndrome; Autism; Excitation; Inhibition; Synaptic plasticity

1. Introduction

ASD[1] encompass sensory and communication disorders, repetitive behaviors, social interaction deficits, increased anxiety, and cognitive impairments. Neuronal information processing that underlies such complex brain functions requires multiple forms of plasticity that have been intensely studied in the CA1 hippocampal region, where a coordinated balance between glutamatergic synaptic excitation mediated by NMDA and AMPA receptors (NMDAR and AMPAR) and GABAergic inhibition mediated by $GABA_A$ receptors ($GABA_AR$) is crucial (E/I balance) (Collingridge et al., 2010; Huganir and Nicoll, 2013; Malenka and Bear, 2004; Oh and Smith, 2019). Whole-exome sequencing to identify genetic differences in individuals with ASD has identified alterations in multiple genes that are important for synaptic development and plasticity (Lu et al., 2012). Of note, genetic alterations associated with ASD and other related neurodevelopmental disorders frequently result in disruptions in synaptic E/I balance in mouse models (Chao et al., 2010; Gogolla et al., 2009; Pizzarelli and Cherubini, 2011; Tabuchi et al., 2007; Zhang et al., 2010). Interestingly, ~30% of individuals with ASD develop clinically apparent seizures with a decrease in the threshold for developing seizures (Brooks-Kayal, 2010; Gillberg and Billstedt, 2000). Additionally, children with ASD exhibit ongoing sharp-spike activity in sleeping EEG or magnetoencephalographic recordings (Lewine et al., 1999; Wheless et al., 2002). Taken together these data suggest that many individuals with ASD develop unstable, hyper-excitable neuronal networks, where there is an imbalance of E/I synaptic transmission that in some cases predisposes to comorbid epilepsy.

Genome-wide association studies and exome sequencing have linked polymorphisms in the genes encoding both the $Ca_V1.2$ and $Ca_V1.3$ LTCC isoforms to increased risk for multiple neurocognitive disorders, including ASD (Bhat et al., 2012; Chao et al., 2010; Lu et al., 2012; Nie et al., 2015; Pinggera and Striessnig, 2016; Smoller et al., 2013). As mentioned above, TS is a rare genetic disorder that in many cases is characterized by a single nucleotide mutation in codon 406 in exon 8 or 8A of the gene encoding the $Ca_V1.2$ LTCC pore-forming subunit (Bader et al., 2011; Bett et al., 2012; Splawski et al., 2004). TS2-neo $Ca_V1.2$ G406R heterozygous knock-in mice, which serve as a model of TS, were generated with an inverted neomycin cassette that lowered the expression of the $Ca_V1.2$

[1] *Non-standard Abbreviations*: Autism spectrum disorder (ASD). Excitation/Inhibition balance (E/I balance), High-frequency stimulation (HFS); L-type calcium channel (LTCC), prolonged theta-train stimulation (PTT), Timothy Syndrome (TS).

G406R mutant from exon 8 via transcriptional interference, thus blunting the full effects of channel gain-of-function, which in the heart can lead to fatal cardiac arrhythmia (i.e. Long QT syndrome 8)(Bader et al., 2011). Behavioral analysis of these animals showed that this single mutation was sufficient to cause phenotypic characteristics that collectively mirror the social interaction deficits, repetitive behaviors, self-injurious overgrooming, heightened anxiety, and cognitive impairments described in ASD (Bader et al., 2011; Bett et al., 2012). Interestingly, a net reduction of dendritic arborization in response to depolarization has been described in the cortex of these animals (Krey et al., 2013), which is similar to observations in the hippocampus of humans with ASD and in induced pluripotent stem cells (iPSC)-derived neurons from patients with TS (Krey et al., 2013). Thus, the overlapping phenotypes reported for the TS2-neo mouse and humans with TS specifically and/or ASD generally make this animal model attractive for the studying how LTCC dysfunction may lead to potential alterations in basal excitatory and inhibitory transmission and synaptic plasticity that could contribute to ASD.

Previous studies recording from TS2-neo mouse cardiomyocytes and heterologous cells expressing the $Ca_V1.2$ G406R mutation are consistent with channel gain-of-function due to increased activation and impaired inactivation leading to long Q-T cardiac arrhythmias (Barrett and Tsien, 2008; Cheng et al., 2011; Dick et al., 2016; Dixon et al., 2012; Navedo et al., 2010; Splawski et al., 2004; Yazawa et al., 2011); however, channel function in neurons remains much less explored. Indeed, it is possible that the relative impacts of the $Ca_V1.2$ G406R mutation may be somewhat different in neurons as compared to other cells due to differences in the expression of $Ca_V1.2$ splice variants, auxiliary subunits, and other regulatory proteins. It was shown in cortical neurons that spontaneous regenerative Ca^{2+} transients mediated by $Ca_V1.2$ G406R channels showed significantly larger spatial spread and amplitude as compared to $Ca_V1.2$ WT, consistent with gain-of-function (Kamijo et al., 2018). Yet, interestingly, this study also found that the duration of Ca^{2+} elevation was shorter compared to WT, thus indicating potentially stronger engagement of negative-feedback mechanisms that limit LTCC Ca^{2+} influx (Kamijo et al., 2018). Yet, another recent study found increased activation of basal transcriptional signaling downstream of $Ca_V1.2$ G406R channels indicative of gain-of-function (Servili et al., 2020). However, neither the impact of the $Ca_V1.2$ G406R mutation on channel function nor on LTCC regulation of synaptic plasticity have been directly examined *in vivo/ex vivo*.

Thus, here we employed the TS2-neo mouse model to characterize the overall impact of the $Ca_V1.2$ G406R mutation *ex vivo* in acute brain slices on channel expression, phosphorylation, and current density, basal AMPAR and NMDAR-mediated excitatory and $GABA_A$R-mediated inhibitory synaptic transmission, and LTCC control of synaptic plasticity in CA1 hippocampal neurons. Importantly, despite normal levels of functional channel expression and basal phosphorylation, we found that TS2-neo mice carrying the $Ca_V1.2$ G406R mutation exhibited slightly increased basal excitatory transmission, strongly decreased basal inhibitory synaptic transmission, and distinct alterations in two different forms of LTCC-dependent (but NMDAR-independent) LTP of excitatory synaptic transmission in CA1 neurons.

2. Materials and methods

2.1. Animal models

All animal procedures were approved by the University of Colorado Anschutz Medical Campus Institutional Animal Care and Use Committee in accordance with National Institutes of Health (NIH)/United States Public Health Service guidelines. Production and initial characterization of TS2-neo mice expressing the $Ca_V1.2$ G406R variant was described in (Bader et al., 2011). TS2-neo mice were obtained from Jackson Laboratories (B6.Cg-Cacna1c$^{tm2Itl/J}$, Strain#:019547; RRID: IMSR_JAX:019547) and maintained as heterozygotes by breeding to WT C57Bl6J. Previous studies identifying ASD-related behavioral phenotypes in TS2-neo mice, including alterations in hippocampal-dependent spatial and contextual fear learning and memory, only analyzed male mice (Bader et al., 2011). In addition, ASD in general is 3–4 times more prevalent in human males than females (Loomes et al., 2017). Thus, in this study we confined our analyses to only male TS2-neo and WT littermate control mice between 8 and 16 weeks of age.

2.2. Whole-cell recordings of synaptic currents in CA1 neurons

For whole-cell, voltage-clamp electrophysiological recordings of excitatory and inhibitory synaptic currents, 300 μm horizontal hippocampal slices were prepared from TS2-neo and WT littermate control mice using a Vibratome as previously done (Sanderson et al., 2016, 2021). After 15 min recovery at 34 °C, slices were then maintained at room temperature until recording. Whole-cell recordings were performed in a chamber maintained at 29–30 °C and visualized using infrared–differential interference contrast microscopy. Patch-clamp electrodes had a resistance between 3 and 6 MΩ. Voltage-clamp recordings were obtained using an Axopatch 200B amplifier using pClamp software (Molecular Devices) at a holding potential of −65 mV, except as noted below for AMPA/NMDA evoked EPSC ratios, AMPAR rectification measurements, and HFS-LTP recordings. No corrections were made for series resistance or liquid junction potentials. AMPAR-mediated sEPSCs isolated using picrotoxin (50 μM; Tocris) were recorded from CA1 pyramidal neurons using an intracellular solution (IS1) containing the following (in mM): 130 Cs gluconate, 1 CsCl, 1 $MgS0_4$, 10 HEPES, 1 EGTA, 4 MgATP, 0.4 MgGTP, and 2 QX-314, pH 7.3. $GABA_A$R-mediated sIPSCs and evoked IPSCs were recorded using an internal solution containing (in mM) 140 CsCl, 10 HEPES, 1 EGTA, 4 MgATP, 0.4 MgGTP, and 2 QX-314, pH 7.3, and were isolated using 2, 3-Dioxo-6-nitro-1,2,3,4-tetrahydrobenzo[*f*]quinoxaline-7-sulfonamide (NBQX 10 μM; Tocris). Evoked GABA IPSC paired-pulse ratios (PPR) assessing pre-synaptic release probability were determined by taking the amplitude ratio of the 2nd IPSC/1st IPSC in response to two stimuli delivered 200 ms apart.

Evoked EPSCs were recorded in whole-cell configuration; half-maximal stimulation was determined and then currents were evoked at holding potentials of −65 mV (inward AMPAR current) or +40 mV (outward AMPAR plus NMDAR current). Averaging recorded events (>10/neuron) and overlaying the traces at −65 mV and +40 was used to determine AMPA/NMDA EPSC ratios as follows: AMPAR currents at +40 or −65 mV measured from the peak amplitude of the EPSC were divided by NMDAR currents at +40 mV measured 70 ms after the onset of the EPSC when the faster AMPAR-mediated component had

decayed. Normalized AMPAR EPSC I–V curves were obtained from averaged recordings (>10/neuron) in the presence of MK-801 (10 μM) and picrotoxin (50 μM) extracellularly and spermine (10 μM) intracellularly. Normalized I–V plots were generated from measurements of AMPAR EPSC peak amplitudes at different membrane holding potentials by dividing the mean AMPAR EPSC peak amplitude determined at −60 mV for each genotype. AMPAR rectification indices (RI) were obtained by dividing the peak amplitudes of AMPAR EPSCs recorded at −60 mV by those recorded at +40 mV for each neuron as indicated.

Whole-cell, voltage-clamp HFS-LTP experiments were recorded from CA1 pyramidal neurons using IS1 containing spermine (10 μM) with MK801 (10 μM) and D-APV (50 μM) present in the ASCF to block NMDARs. A bipolar tungsten-stimulating electrode was placed in the SC pathway 200 μm from the CA1 pyramidal cell body to evoke AMPAR EPSCs recorded at ~−40 mV where little or no net $GABA_AR$ inward or outward current is present. After establishing whole-cell access, a 3 min gap-free baseline recording at ~−40 mV was performed. HFS-LTP was then induced using a pairing protocol; cells were depolarized to 0 mV and held there for 90 s, with a pulse every 20 s, LTP was subsequently induced by additional delivery of 2 × 100Hz HFS, 1s trains separated by 20 s. The neuron was then returned to ~ −40 mV and evoked EPSC amplitudes were subsequently monitored every 20 s. Similar recording approaches were used to assess the impacts of blocking LTCCs with nimodipine (10 μM) and $GABA_ARs$ with picrotoxin (50 μM) on this HFS-LTP.

2.3. Whole-cell recordings of voltage-gated Ca^{2+} currents in CA1 neurons

Voltage-gated Ca^{2+} currents were recorded in whole-cell patch clamp configuration using an Axopatch 200B amplifier using pClamp software (Molecular Devices), with the above-described internal solution also containing 10 mM QX-314, 10 μM spermine, 10 mM tetraethylammonium chloride, and 2 mM 4-aminopyridine. The extracellular ASCF contained tetrodotoxin (1 μm), 10 mM tetraethylammonium chloride, 50 μM picrotoxin, 10 μM NBQX, 10 μM MK801, and 50 μM D-APV. I–V curves were generated in response to 500 ms step depolarizations from a holding potential of −60 mV in 10 mV increments from −50 to +20 mV in the absence and then the presence of 10 μM nimodipine to determine LTCC contributions. Leak currents were measured at −50 mV and then proportionally subtracted from the evoked voltage-gated Ca^{2+}currents (I_{Ca}) as a linear function of increasing membrane voltage for each depolarizing step from −60 to +20 mV.

2.4. Extracellular fEPSP recordings

Unless indicated, all chemicals were from Sigma-Aldrich. For slice preparation, 8-16 week-old mice were decapitated under deep anesthesia with isoflurane via inhalation, prior to decapitation and then the brain was removed into 4 °C cutting solution (in mM: 3 KCl, 1.25 $NaH2PO_4$, 12 $MgSO_4$, 26 $NaHCO_3$, 0.2 $CaCl_2$, 220 sucrose, 10 glucose) as done previously (Sanderson et al., 2021). The hippocampi were removed from the brain, and 400-μm-thick horizontal slices were made using a McIIwain tissue chopper. Slices were recovered at 27 °C for >90 min in ACSF/cutting solution mixture (ACSF in mM: 126 NaCl, 5 KCl, 2 $CaCl_2$, 1.25 NaH_2PO_4, 1 $MgSO_4$, 26 $NaHCO_3$, 10 glucose, and 2 *N*-acetyl cysteine). Following recovery, slices were transferred to a recording chamber and maintained at 29–31 °C in ACSF minus *N*-acetyl cysteine. A bipolar tungsten stimulating electrode was placed in the

SC pathway 200–300 μm from CA1 cell bodies to evoke fEPSPs recorded in the stratum radiatum using a nearby glass micropipette filled with ACSF (access resistance, 2–5 MΩ). Input-output (I–O) curves were measured by evoking fEPSPs at different intensities until the maximal response was determined by plotting initial fEPSP slope against stimulus intensity. PPR assessing pre-synaptic glutamate release probability was determined by taking the amplitude ratio of the 2nd fEPSP/1st fEPSP (x100) in response to two stimuli delivered 50 ms apart. For studies of prolonged theta tetanus (PTT)-LTP, the test stimulus intensity was set to evoke 40–60% of the maximum slope and delivered at 0.05 Hz, then 5 Hz stimulation was applied for 3 min and fEPSP responses were followed for another 45 min. When examining β-adrenergic regulation of PTT-LTP, isoproterenol bitartrate (3 μM) was bath-applied for 10 min prior to PTT stimulation. Scope54 or WinLTP software was used for data acquisition and analysis.

2.5. Immunoblotting of hippocampal homogenates

Hippocampal slices were prepared using a vibratome and recovered as for electrophysiology with the addition of cuts to isolate CA1 from the remaining hippocampus; after recovery, the slices were suspended in 100 μl 1%Triton X-100 lysis buffer (1% Triton X-100, 150 mM NaCl,10 mM EDTA, 10 mM EGTA, 10 mM Tris pH 8.0) plus a protease and phosphatase inhibitor cocktail (Thermo scientific #1861281) for each 10 mg of tissue, sonicated in buffer with 5x loading dye added, and boiled for 5min. For immunoblotting, 20 μl of this whole hippocampal slice homogenate was resolved on 7.5% Tris-SDS polyacrylamide gels and transferred in 7.5% methanol to PVDF membranes. Blots were blocked in Tris-buffered saline (TBS; 140 mm NaCl, 20 mm Tris pH 7.6) plus 1% BSA overnight at 4 °C and then cut in half at ~150 kDa to allow separate probing of the top half of the blots to measure phospho-S1928 levels (rabbit anti-$Ca_V1.2$P–S1928; provided by William Catterall, University of Washington ((De Jongh et al., 1996); 1:500) followed by total $Ca_V1.2$ expression (rabbit anti-$Ca_V1.2$; Alomone Laboratories ACC-003; 1:200) and the bottom half of the blot for β-actin (rabbit anti-β-actin; Cell Signaling #4967; 1:1000) to allow normalization of total $Ca_V1.2$ expression to β-actin as a protein loading control for each lane (see Supplemental Fig. 1). For $Ca_V1.2$ *P*–S1928 analysis, WT and TS2-neo samples were run side-by-side on the same gel/blot and processed as in (Murphy et al., 2014). Briefly, blots were probed with rabbit anti-$Ca_V1.2$P–S1928 for 1 h at room temperature before visualization (described below) followed by stripping (200 mM glycine buffer pH 2.7, 2 × 10 min) and re-probing overnight at 4 °C with rabbit anti-$Ca_V1.2$ (Alomone Laboratories ACC-003; 1:200) to allow normalization to total channel levels. After primary antibody incubations, blots were subjected to three 10-min washes in TBS plus 0.1% Tween 20 (TTBS), before being incubated with anti-rabbit HRP-coupled secondary antibody (Bio-Rad; 1:5000) in 1% BSA for 1 h at room temperature, followed by three additional 10-min washes in TTBS. Immunodetection visualization was accomplished using a chemiluminescent substrate kit (SuperSignal West Femto Maximum Sensitivity Substrate; Pierce) and the Alpha Innotech (Alpha Innotech, San Leandro, CA, USA) imaging system. Quantification was performed using AlphaEase software (Alpha Innotech, San Leandro, CA, USA) and Excel (Microsoft, Redmond, WA, USA).

2.6. Quantification and statistical analyses

fEPSP slope and amplitude measurements and analyses were made using WinLTP or Scope54. Whole-cell current measurements and analyses were performed using in Clampfit (for evoked EPSCs, IPSCs and Ca^{2+} currents) and Mini-Analysis (for sEPSCs and sIPSCs). LTP time-course data, I–V curves, and I–O curves were analyzed using standard two-way ANOVA in Prism (GraphPad). Datasets were tested for normality using either the Kolmogorov-Smirnov or D'Agostino and Pearson normality tests in Prism. Pairwise comparisons for normally distributed data were by unpaired, two-tailed *t*-test in Prism. Pairwise comparisons for non-normally distributed data were by Mann-Whitney, two-tailed test in Prism. sEPSC and sIPSC amplitude and inter-event interval raw values used to generate cumulative distribution plots were analyzed using the Kolmogorov-Smirnov (K–S) test in Prism. Significance is reported as *p < 0.05 and data are presented as mean ± SEM. In most cases, were possible, the raw data points are also represented on the graphs. Actual p values are reported in the Results text when provided by the software. When actual p values are not provided by the software only *p < 0.05, **p < 0.01, **p < 0.001, and ****p < 0.0001 are reported in the Results text. Only *p < 0.05, **p < 0.01, **p < 0.001, and ****p < 0.0001 are reported in the Figure Legends. p > 0.05 is reported as ns (not significant).

3. Results

3.1. Basal excitatory synaptic input to CA1 neurons is slightly increased in TS2-neo mice

Prior research identified multiple ASD-related behavioral phenotypes in male TS2-neo mice, including alterations in hippocampal-dependent spatial and contextual fear learning and memory (Bader et al., 2011). Thus, here we first used whole-cell voltage-clamp recording to characterize basal synaptic inputs onto hippocampal CA1 neurons in young adult (8-16 weeks-old) male TS2-neo and WT littermate control mice. Recordings of AMPAR-mediated spontaneous excitatory postsynaptic currents (sEPSCs) at a holding potential of −65 mV, in the presence of picrotoxin (50 μM) to block $GABA_A$Rs (Fig. 1A), revealed that TS2-neo mice exhibited a small, but significant increase in mean sEPSC amplitude (Fig. 1B; WT 11.3 ± 0.6 pA n = 16 cells, 4 animals, TS2-neo 15.5 ± 1.6 n = 15 cells, 5 animals; *p = 0.018 by *t*-test) and a clear rightward-shift in the cumulative distribution of sEPSC amplitudes (****p < 0.0001 by K–S test; Fig. 1C) compared to WT. In addition, while sEPSC rise time kinetics were not different between WT and TS2-neo (Supplemental Fig. 1A), sEPSC decay time was slightly increased in TS2-neo compared to WT (Supplemental Fig. 1B), which can also increase the effective strength of excitatory input by prolonging postsynaptic depolarization (Hansen et al., 2021). However, there was no significant difference in the mean frequency of sEPSC events (Fig. 1D; WT 0.9 ± 0.2 Hz n = 16 cells, 4 animals, TS2-neo 0.7 ± 0.2 HZ n = 15, 5 animals; p = 0.19 by *t*-test), yet there was a small, but significant rightward shift in the cumulative distribution of interevent intervals, indicating a modest decrease in the frequency of excitatory synaptic events for TS2-neo compared to WT (Fig. 1E; ****p < 0.0001 by K–S test). These data indicate that the overall basal strength of individual excitatory synaptic inputs to CA1 neurons is somewhat increased in TS2-neo mice, but this increase in synaptic strength is partially offset by a slight decrease in the frequency of synaptic events.

We then assessed the ratio of evoked AMPAR to NMDAR-mediated basal synaptic transmission in response to stimulation of the Schaffer collateral (SC) inputs from CA3, with the amplitude of the fast, evoked AMPAR EPSC measured as the peak of the inward response recorded at −60 mV and the amplitude of the slow, evoked NMDAR EPSC measured 70 ms after the onset of the outward response recorded +60 mV, when the faster AMPAR-mediated component had decayed (Fig. 1F; Supplemental Fig. 1C). These measurements determined that neither normalized AMPA/NMDA EPSC ratios (Fig. 1G; WT 5.6 ± 1.0 n = 16 cells, 4 animals, TS2-neo 5.5 ± 1.0 n = 8 cells, 3 animals; p = 0.95 by *t*-test) nor mean amplitudes of NMDA EPSC responses (Fig. 1H; WT 54 ± 8 pA n = 14 cells, 4 animals, TS2-neo 39 ± 10 pA n = 7 cells, 3 animals; p = 0.22 by *t*-test) were different in TS2-neo compared to WT mice. In addition, the decay time of the slow, NMDAR-mediated component of outward +60 mV EPSC response was not different for TS2-neo compared to WT mice (Supplemental Fig. 1D).

We previously demonstrated that recruitment of the cAMP-dependent protein kinase A (PKA) and the Ca^{2+}-dependent protein phosphatase calcineurin (CaN) to LTCCs by the postsynaptic scaffold protein A-kinase anchoring protein (AKAP) 79/150 prominently regulates basal LTCC current density and Ca^{2+}-dependent inactivation in hippocampal neurons. In particular, genetic disruption of CaN anchoring to AKAP79/150 led to LTCC gain-of-function by inhibiting Ca^{2+}-dependent inactivation that is primed by PKA signaling (Dittmer et al., 2014; Oliveria et al., 2012). However, this same genetic disruption of CaN anchoring to AKAP79/150 that increased neuronal LTCC function also aberrantly increased the basal CA1 synaptic incorporation of GluA1 subunit homomeric Ca^{2+}-permeable AMPARs (CP-AMPAR) subunits (Sanderson et al., 2012, 2016, 2021). These GluA2-lacking CP-AMPARs can be distinguished by inward-rectification on current-voltage (I–V) plots due to the block of outward current through these channels by intracellular polyamines (Hansen et al., 2021; Purkey and Dell'Acqua, 2020). Thus, to determine whether $Ca_V1.2$ G406R gain-of-function mutation that prevents LTCC inactivation (Barrett and Tsien, 2008; Dick et al., 2016) might also lead to alterations in synaptic AMPAR subunit composition, we measured evoked AMPAR EPSCs over range of membrane holding potential from −60 to +60 mV. The resulting normalized AMPA EPSC I–V plots showed a small decrease in outward AMPA EPSC amplitudes indicative of slightly increased AMPAR inward rectification in TS2-neo mice (Fig. 1I; *p < 0.05 by 2-way ANOVA). However, parallel measurements of AMPA −60 mV/+40 mV EPSC rectification indices (RI) did not show a significant difference between TS2-neo and WT (Fig. 1J; WT 2.4 ± 0.4 n = 16 cells, 4 animals; TS2-neo 2.8 ± 0.5 n = 8 cells, 3 animals; p = 0.52 by *t*-test).

CP-AMPARs also exhibit faster kinetics (both rise and decay times) compared to GluA2-containing AMPARs (Hansen et al., 2021); however, as noted above, sEPSC rise times were not different between WT and TS2-neo (Supplemental Fig. 1A) and sEPSC decay time was slightly slower for TS2-neo (Supplemental Fig. 1B). In addition, no significant difference in the decay times of evoked AMPA EPSCs were found for TS2-neo compared to WT (Supplemental Fig. 1C). As small changes in AMPAR EPSC rectification and decay kinetics can also result from the presence of different auxiliary subunits and GluA subunit alternative splicing changes (Hansen et al., 2021), synaptic AMPAR subunit composition is likely to be for the most part unchanged at SC-CA1 synapses in TS2-neo mice. However, we cannot

completely rule out a small increase in the basal incorporation of CP-AMPARs that, due their higher single-channel conductance, could be in part contributing to the increase in sEPSC amplitude observed above (Fig. 1B and C).

3.2. Basal inhibitory synaptic input to CA1 neurons is decreased in TS2- neo mice

In order to determine whether GABAergic inhibition is altered in TS2-neo mice, we recorded $GABA_AR$-mediated spontaneous inhibitory postsynaptic currents (sIPSCs) at a holding potential of −65 mV in the presence of NBQX (10 μM) to block AMPARs (Fig. 2A) and found that TS2-neo exhibited a significant decrease in mean sIPSC amplitude (Fig. 2B; WT 30 ± 1.4 pA n = 16 cells, 5 animals, TS2-neo 25 ± 1.7 n = 12 cells, 5 animals; *p = 0.021 by *t*-test) and a clear leftward-shift in the cumulative distribution of sIPSC amplitudes compared to WT mice (**p = 0.0059 by K–S test; Fig. 2C). In addition, there was a large decrease in the mean frequency of sIPSC events (Fig. 1D; WT 6.2 ± 0.8 Hz n = 16, 5 animals; TS2-neo 2.6 ± 0.5 HZ n = 12, 5 animals; **p = 0.0024 by *t*-test) and a prominent rightward shift in the cumulative distributions of interevent intervals for TS2-neo compared to WT mice (****p < 0.0001 by K–S test; Fig. 2E). In addition, both the sIPSC rise times (Fig. 2F; WT 3.3 ± 0.2 ms, n = 17 cells, 5 animals, TS2-neo 4.2 ± 0.3 ms n = 13 cells, 5 animals; **p = 0.0016 by *t*-test) and decay times (Fig. 2G; WT 4.6 ± 0.2 ms n = 17 cells, 5 animals, TS2-neo 5.6 ± 0.3 ms n = 13 cells, 5 animals; *p = 0.017 by Mann-Whitney test) were slightly increased for TS2-neo compared to WT. These slower sIPSC kinetics in TS2-neo could reflect changes in postsynaptic $GABA_AR$ subunit composition and/or accessory proteins (Han et al., 2021). Regardless, the profound decrease in sIPSC frequency we observe in TS2-neo could be indicative of decreased presynaptic GABA release. Thus, to independently assess GABA release onto CA1 neurons, we measured paired-pulse ratios (PPR), which are inversely related to release probability, for evoked GABA-mediated IPSCs in response to two stimuli delivered in stratum radiatum 200 ms apart (Fig. 1F). Consistent with decreased probability of GABA release in TS2-neo mice, GABA PPR was significantly increased in TS2-neo compared to WT (Fig. 1G; WT 0.62 ± 0.03 n = 12 cells, 3 animals; TS2-neo 0.74 ± 0.02 n = 7 cells, 3 animals; *p = 0.011 by *t*-test). Thus, these data indicate that basal inhibitory input to CA1 neurons is substantially decreased in TS2-neo mice, and when combined with slightly increased excitatory transmission observed, indicate that overall CA1 neuron synaptic E/I balance is likely shifted toward excitation.

3.3. LTCC-dependent HFS-LTP at CA1 synapses is impaired in TS2-neo mice

Various patterns of high-frequency stimulation (HFS) can induce LTP at SC-CA1 synapses that depends on Ca^{2+} influx through NMDARs, LTCCs, or a combination of both (Moosmang et al., 2005). In addition, given the decreased basal GABAergic input to CA1 neurons in TS2-neo mice described above, we wanted to assess impacts of the $Ca_V1.2$ G406R mutation on LTP, not only under conditions that depend on LTCCs, but also where GABAergic inhibition is left unblocked. To this end, we first monitored inward evoked SC-CA1 AMPAR EPSC responses at a holding potential of ~ −40 mV (where little or no inward or outward $GABA_AR$ current is present) and then induced LTP in the presence of NMDAR blockers (MK801, D-APV) by delivering 2 × 100 Hz, 1 s HFS trains spaced 20 s apart paired with current injection to depolarize the postsynaptic neuron to 0 mV. We then returned to ~ −40 mV to monitor AMPAR EPSC responses post-induction and found that

this 2 × 100Hz HFS protocol reliably induced LTP of AMPAR EPSC responses in WT slices (Fig. 3A and B). Importantly, induction of this NMDAR-independent HFS-LTP was blocked both by the LTCC antagonist nimodipine (WT control n = 14 cells, 12 animals; +nimodipine 10 μM n = 6 cells, 5 animals; ****p < 0.0001 by two-way ANOVA last 10 min) and also by the $GABA_AR$ antagonist picrotoxin (+picrotoxin 50 μM n = 11 cells, 11 animals; ****p < 0.0001 by two-way ANOVA last 10 min) (Fig. 3A and B). Interestingly, this LTCC-dependent, GABAR-dependent HFS-LTP was also strongly impaired in slices from TS2-neo mice (Fig. 3C and D; WT n = 14 cells, 12 animals; TS2-neo n = 6 cells, 5 animals; ****p < 0.0001 by two-way ANOVA last 10 min). These findings could indicate, that despite the $Ca_V1.2$ G406R mutation causing biophysical gain-of-function at the single channel level, *in vivo* there could actually be some sort of compensatory down-regulation of overall LTCC function in TS2-neo mice. However, given the additional dependence of this HFS-LTP on $GABA_AR$ activity, this impairment in TS2-neo mice could also be related to the decreased basal GABAergic inhibition reported above (Fig. 2).

3.4. $Ca_V1.2$ expression, basal phosphorylation, and LTCC current density in CA1 neurons is not altered in TS2-neo mice

To determine whether any negative-feedback, compensatory mechanism might be engaged in TS2-neo mice to somehow decrease overall LTCC expression and function, we first assessed overall $Ca_V1.2$ expression in CA1 hippocampus by immunoblotting, and found no difference for $Ca_V1.2$ protein levels normalized to β-actin in TS2-neo compared to WT (Fig. 4A and B; WT 0.09 ± 0.03, n = 7 animals; TS2-neo 0.09 ± 0.02, n = 8 animals; p = 0.96 ns by *t*-test). We and others previously found that PKA phosphorylation of $Ca_V1.2$ at Ser1928 in the distal C-terminus plays a prominent role in maintaining basal LTCC activity and also allowing further enhancement in response to β-adrenergic receptor stimulation in hippocampal neurons (Murphy et al., 2014; Patriarchi et al., 2016; Qian et al., 2017). Thus, we next measured the basal levels of $Ca_V1.2$ S1928 phosphorylation by immunoblotting and found no difference in phospho-S1928 immunoreactivity normalized to total $Ca_V1.2$ immunoreactivity in hippocampal slice homogenates from TS2-neo compared to WT mice (Fig. 4A,C; WT 0.18 ± 0.04, n = 7 animals; TS2-neo 0.17 ± 0.03, n = 8 animals; p = 0.86 ns by *t*-test).

Finally, we used whole-cell recording in CA1 neurons to measure voltage-gated Ca^{2+} current density (i.e. I_{Ca} in pA normalized to cell capacitance in pF, which is proportional to cell size and was found to be similar for WT (202 ± 51 pF) and TS2-neo (214 ± 21 pF); p = 0.81 ns by *t*-test), in response to a series of 500 ms step depolarizations from −60 to +20 mV (Fig. 4D). While these measurements made 250 ms after initiating depolarization (i.e. in the middle of each 500 ms step depolarization) are somewhat inexact due to the inability to fully clamp membrane voltage in these large, mature, dendritically complex neurons, plotting I_{Ca} density versus voltage (I–V curve) revealed no significant differences between WT and TS2-neo (Fig. 4F; WT n = 6 cells, 3 animals; TS2-neo n = 13 cells, 5 animals; p > 0.05, ns by two-way ANOVA). To more specifically investigate the contribution of LTCCs to total I_{Ca} density, nimodipine (10 μM) was then added and I_{Ca} density measurements were repeated for the same cells (Fig. 4E). Importantly, nimodipine reduced I_{Ca} density similarly in both WT and TS-neo neurons with the resulting post-nimodipine I–V curves not being

significantly different (Fig. 4G; WT n = 6 cells, 3 animals; TS2-neo n = 13 cells, 5 animals; $p > 0.05$, ns by two-way ANOVA). In addition, despite the G406R mutation previously being linked to impaired channel inactivation, we detected no significant differences in the apparent kinetics of inactivation of I_{Ca} measured as decay slope following depolarization to −10 mV in either the absence (Fig. 4H; WT 5.7 ± 2.1 pA/ms n = 6 cells, 3 animals; TS2-neo 8.4 ± 1.1 pA/ms n = 13 cells, 5 animals; $p = 0.18$ ns by Mann-Whitney test) or presence of nimodipine (Fig. 4I; WT + Nim 4.3 ± 1.2 pA/ms n = 6 cells, 3 animals; TS2-neo + Nim 5.8 ± 0.9 pA/ms n = 13 cells, 5 animals; $p = 0.43$ ns by Mann-Whitney test). Thus, we can infer that the LTCC contributions to total voltage-gated Ca^{2+} current in CA1 neurons are roughly similar in WT and TS2-neo mice and that no unexpected, compensatory global down-regulation of LTCC function resulted from chronic expression of the G406R gain-of-function mutant.

3.5. TS2-neo mice are sensitized to induction of LTP by prolonged theta-train stimulation

Lastly, we used extracellular recordings of field excitatory postsynaptic potentials (fEPSP) evoked by stimulation of SC inputs to CA1 neuron dendrites in stratum radiatum to assess another form of LTCC-dependent LTP that in WT mice requires 5 Hz prolonged theta-train (PTT) stimulation in the presence of a β-adrenergic receptor agonist to promote PKA signaling-mediated enhancement of LTCC activity. Importantly, this PTT-LTP is completely inhibited by LTCC antagonists (but not NMDAR antagonists) and is absent in both forebrain-restricted $Ca_V1.2$ knock-out mice and phosphorylation-deficient $Ca_V1.2$ S1928A knock-in mice (Patriarchi et al., 2016; Qian et al., 2012, 2017; Zhang et al., 2013). But first, to control for any possible confounding differences in basal AMPAR transmission, we determined input-output (I–O) relationships measuring fEPSP slope for range of stimulus intensities (Fig. 5A) and PPR, as a relative measure of presynaptic glutamate release probability (Fig. 5B), but found no significant differences in either set of measurements (Fig. 5A; I-0 WT n = 9, 26, 15,10, 6; TS2-neo n = 10, 28, 23, 24, 5; $p > 0.05$ ns by two-way ANOVA; Fig. 5B; PPR 146 ± 8 WT n = 10; TS2-neo 159 ± 7 n = 9; $p = 0.24$ ns by test).

In agreement with prior studies of PTT-LTP mentioned above, delivery of 5 Hz PTT for 3 min in WT control slices resulted in a brief potentiation followed by a transient depression that then recovered back to baseline after PTT stimulation was terminated, with no resulting net change in synaptic strength observed after ~30–45 min (Fig. 5C and D). However, when 5 Hz PTT stimulation was instead delivered following application of the β-adrenergic agonist isoproterenol (Iso, 3 μM) substantial potentiation (~30%) of the fEPSP response resulted within ~30–45 min (Fig. 5C and D; WT Control n = 9 slices, 9 animals; WT + Iso n = 12 slices, 11 animals; ****$p < 0.0001$ by two-way ANOVA last 10 min). Consistent with prior studies demonstrating that PPT-LTP is LTCC-dependent, treatment with nimodipine (10 μM) prevented Iso from promoting any significant potentiation in response to 5 Hz PTT stimulation (Fig. 5D; WT + Iso + Nim n = 4 slices, 4 animals; ****$p < 0.0001$ by two-way ANOVA last 10 min compared to WT + Iso; $p = 0.17$ ns by two-way ANOVA last 10 min compared to WT Control).

Interestingly, 5 Hz PTT stimulation following Iso application also resulted in substantial fEPSP potentiation (~30%) in slices from TS2-neo mice (Fig. 5E and F) that was

indistinguishable from the level of potentiation seen in W + Iso slices (Fig. 5H; TS2-neo + Iso, n = 14 slices, 13 animals; p = 0.93 ns by two-way ANOVA last 10 min compared to WT + Iso). In contrast, stimulation of TS2-neo slices under control conditions with 5 Hz PTT alone resulted in measurable levels of potentiation (~12%) that, while significantly less than those observed for TS2-neo slices treated with Iso (Fig. 5F; TS2-neo Control n = 10 slices, 10 animals; TS2-neo + Iso, n = 14 slices, 13 animals; ***p = 0.0002 by two-way ANOVA last 10 min), were significantly above those seen for WT control conditions with 5 Hz PTT alone (Fig. 5G; TS2-neo control n = 10 slices, 10 animals; *p = 0.033 by two-way ANOVA last 10 min compared to WT Control). Thus, the $Ca_V1.2$ G406R mutation in TS2-neo appears to be sensitizing CA1 synapses to induction of LTP by 5 Hz PTT stimulation alone, which then partially occludes some of the additional potentiation resulting from PTT stimulation in presence of Iso. These findings for 5 Hz PTT-LTP in TS2-neo mice, unlike those above for 2 × 100 Hz HFS-LTP, are more readily consistent with LTCC gain-of-function as expected for the G406R mutant. Congruent with this possible linkage to LTCC gain-of-function, incubation with nimodipine prevented potentiation in response to 5 Hz PTT stimulation alone in TS2-neo mice (Fig. 5I; TS2-neo Control + Nim n = 5 slices, 5 animals; ***p = 0.0002 by two-way ANOVA last 10 min compared to TS2-neo Control).

4. Discussion

4.1. LTCC regulation of excitatory and inhibitory synaptic development and plasticity

Plasticity at hippocampal excitatory and inhibitory synapses is required for normal learning and memory (Collingridge et al., 2010; Huganir and Nicoll, 2013; Malenka and Bear, 2004; Oh and Smith, 2019), and plasticity alterations are frequently observed in rodent models of human brain disorders, including Alzheimer's, Down syndrome, schizophrenia, and ASD (Bozdagi et al., 2010; Choong et al., 2015; Liu et al., 2011; Silverman et al., 2010; Smith and Kittler, 2010; Zhou et al., 2016). NMDARs and LTCCs each activate signaling pathways controlling both rapid changes at synapses that occur within sec-min of plasticity induction as well as subsequent long-lasting changes in gene expression that are required to maintain plasticity expression over hrs-days (Catterall, 2011; Dolmetsch, 2003; Greer and Greenberg, 2008; Grover and Teyler, 1990; Langwieser et al., 2010; Moosmang et al., 2005; Rajgor et al., 2020; Wild et al., 2019). In particular, during plasticity induction membrane depolarization generated by NMDARs and AMPARs can open LTCCs to mediate rapid Ca^{2+}-dependent signaling events controlling postsynaptic AMPAR and $GABA_AR$ trafficking, LTP expression, and structural remodeling of dendritic spines (Dittmer et al., 2017, 2019; Garcia et al., 2021; Hiester et al., 2017; Moosmang et al., 2005; Qian et al., 2012, 2017), as well as long-term changes in gene transcription that support plasticity maintenance (Deisseroth et al., 1996; Graef et al., 1999; Kang et al., 2001; Li et al., 2012, 2016; Ma et al., 2014; Mermelstein et al., 2000; Murphy et al., 2014, 2019; Oliveria et al., 2007; Rajgor et al., 2020; Wheeler et al., 2008, 2012; Wild et al., 2019; Wu et al., 2001).

The $Ca_V1.2$ and $Ca_V1.3$ LTCC pore forming subunits are both expressed in the brain, with $Ca_V1.2$ present at higher levels in hippocampal neurons, where it localizes in the soma, dendrites, and dendritic spines (Di Biase et al., 2008, 2011; Obermair et al., 2004). Accordingly, forebrain-specific $Ca_V1.2$ knockout mice exhibit impairments in learning and

memory and hippocampal LTP (Moosmang et al., 2005). Given the central role of LTCCs in regulating plasticity, it is also not surprising that polymorphisms in the *CACNA1C* gene that are thought to impact $Ca_V1.2$ expression have been linked to ASD, schizophrenia, depression, and bipolar disorder (Bhat et al., 2012; Smoller et al., 2013). In addition, we have observed increased LTCC function in concert with ASD-related behavioral phenotypes and altered CA1 hippocampal synaptic plasticity after early life seizures in rats (Bernard et al., 2014, 2015). As introduced above, rare gain-of-function mutations in *CACNA1C* (Barrett and Tsien, 2008; Dick et al., 2016; Dixon et al., 2012; Erxleben et al., 2006; Li et al., 2016; Limpitikul et al., 2016; Navedo et al., 2010) and *CACNA1D* (the gene encoding $Ca_V1.3$) are linked to TS-associated ASD and non-syndromic ASD, respectively (Pinggera et al., 2015; Splawski et al., 2004).

4.2. Disruption of E/I balance and HFS-LTP by expression of the $Ca_V1.2$ G406R TS mutation

A prominent feature of all of the nervous system disorders mentioned above, including ASD, is altered neuronal excitability and synaptic plasticity related to disruption of synaptic E/I balance (Smith and Kittler, 2010). Importantly, here using a TS2-neo mouse model that expresses one copy of the $Ca_V1.2$ G406R gain-of-function mutation and exhibits social interaction deficits, repetitive behaviors, and hippocampal-dependent cognitive impairments mirroring ASD (Bader et al., 2011), we found alterations in both basal excitatory and inhibitory transmission and synaptic plasticity at CA1 hippocampal synapses. In particular, the basal level of GABAergic synaptic input onto hippocampal CA1 neurons was strongly reduced while the basal level of glutamatergic synaptic input was somewhat increased, which could be consistent with an overall net shift in E/I balance toward excitation. While the underlying mechanism by which the $Ca_V1.2$ G406R gain-of-function mutation is leading to reduced GABAergic inhibition remains to be determined, the decrease in sIPSC amplitude could involve changes in synaptic development downstream of alterations in LTCC regulation of transcriptional signaling pathways that are known to control $GABA_AR$ expression both directly and indirectly (Oh and Smith, 2019; Quadrato et al., 2014; Rajgor et al., 2020).

The even larger decrease in sIPSC frequency in TS2-neo mice, which we were able to at least in part link to decreased presynaptic GABA release, could be related to decreased retrograde communication from CA1 pyramidal cells to presynaptic interneurons via brain-derived neurotrophic factor, an activity-dependent gene product whose expression is known to be controlled by LTCC-dependent transcriptional signaling and to regulate presynaptic GABAergic properties and E/I balance (Belfield et al., 2006; Greer and Greenberg, 2008; Guzikowski and Kavalali, 2022; Peng et al., 2010; Singh et al., 2006). In addition, studies in TS2-neo mice and iPSC-derived cerebral organoids from patients with TS have both identified impairments in cortical interneuron migration that could also contribute to decreased inhibition (Birey et al., 2022; Horigane et al., 2020). Thus, we cannot rule out additional direct contributions of $Ca_V1.2$ G406R mutant expression in presynaptic interneurons. Another, but not mutually exclusive, possibility is that reduced dendritic arborization caused by expression of the G406R mutation (Kamijo et al., 2018; Krey et al., 2013) could be leading to a corresponding reduction in the total number of excitatory

synapses that then triggers compensatory homeostatic plasticity that scales-up excitatory synaptic strength (as seen in Fig. 1A-C) but scales down inhibitory synaptic strength (as seen in Fig. 2A-E) to maintain some basal target level of neuronal firing (Turrigiano, 2012). However, our measurements of cell capacitance, while lacking in precision due to poor voltage-clamp, are not consistent with any major differences in CA1 pyramidal cell size between WT and TS2-neo mice.

Regardless, we were able to potentially link loss of synaptic inhibition in TS2-neo mice to a profound disruption of LTCC-dependent HFS-LTP that also requires intact GABAergic inhibition for its induction. While it is not entirely clear what role $GABA_A$Rs are playing to support induction of this LTCC-dependent LTP in WT neurons, one possibility is that by pairing HFS with depolarization to 0 mV we are allowing feed-forward inhibition onto CA1 neurons to instead produce outward, depolarizing excitatory Cl-currents through synaptic $GABA_A$Rs to assist in driving LTCC opening and Ca^{2+} influx that then activates signaling pathways required for AMPAR potentiation. Indeed, during early postnatal development GABA is excitatory due to high $[Cl^-]_{internal}$, and the excitatory actions of $GABA_A$R activation promote LTCC opening that controls the development and strengthening of both inhibitory and excitatory synapses to establish E/I balance in the hippocampus and other brain regions (Ben-Ari, 2002, 2014; Ben-Ari et al., 2007; Caillard et al., 1999; McLean et al., 1996; Oh and Smith, 2019; Sanderson et al., 2012; Zucca and Valenzuela, 2010). Thus, the reduced GABAergic synaptic transmission in TS2-neo CA1 neurons may be insufficient to drive enough LTCC opening to induce this form of HFS-LTP, despite the channel gain-of-function conferred by the G406R mutation. Accordingly, changes in how LTCCs respond to depolarizing GABA-mediated excitation, and also in turn regulate GABAergic synaptic plasticity and development, could be intertwined in a manner such that both are altered in TS2-neo mice due to chronic expression of the G406R mutation.

4.3. Partial mimicking and occlusion of β-adrenergic receptor-mediated PTT-LTP by expression of the $Ca_V1.2$ G406R TS mutation

In addition to the complicated interplay between LTCCs and GABAergic synaptic development discussed above that could be responsible for disruption of HFS-LTP induction, it was possible that compensatory, negative feedback mechanisms, such as STIM1 activation that triggers $Ca_V1.2$ inhibition, endocytosis and down-regulation of expression (Dittmer et al., 2017; Park et al., 2010; Wang et al., 2010), could have been engaged by chronic expression of the gain-of-function G406R mutant, ultimately leading to paradoxical loss-of-function. However, neither immunoblotting to measure total $Ca_V1.2$ expression levels nor electrophysiology to assess LTCC contributions to voltage-gated Ca^{2+} current density provided any evidence for chronic negative feedback-mediated down-regulation of LTCC function in TS2-neo mice. That overall $Ca_V1.2$ expression levels were unchanged in TS2-neo mice is interesting given that the G406R mutant allele is known to be transcribed at lower levels than the WT allele in these heterozygous mice (Bader et al., 2011). Thus, increased expression of the WT allele may be maintaining $Ca_V1.2$ expression and LTCC current density in TS2-neo mice. Interestingly, there was also no significant difference in the apparent kinetics of inactivation of I_{Ca} in TS2-neo versus WT CA1 neurons; however, once again greater expression of the WT $Ca_V1.2$ allele in TS2-neo mice, the contributions of other

non-L-type high-voltage-activated Ca^{2+} channels to the recorded currents, and the inability to adequately clamp membrane voltage in these large neurons limits our ability to interrogate meaningful differences in channel kinetics. In addition, it is possible that the prominent expression of the Stac (Src homology 3 and cys-enriched domains) adaptor proteins in adult forebrain, which suppress Ca^{2+}-dependent inactivation of WT $Ca_V1.2$ in heterologous systems and of endogenous LTCC currents in neurons, could also be minimizing any potential observable differences in inactivation between TS2-neo and WT mice (Campiglio et al., 2018; Polster et al., 2018).

In addition, we found no change for TS2-neo mice in the basal level of phosphorylation of $Ca_V1.2$ on Ser1928, a site that both helps maintain basal LTCC activity (Murphy et al., 2014; Oliveria et al., 2007) and is required for enhancement of neuronal LTCC activity by β-adrenergic receptor-PKA signaling that promotes PTT-LTP in hippocampal neurons (Qian et al., 2017). To this end, we showed that the maximal ability of the β-adrenergic receptor agonist Iso to promote PTT-LTP at CA1 synapses was similar in WT and TS2-neo neurons. However, we found in contrast to WT, PTT stimulation alone produced significant potentiation at TS2-neo CA1 synapses that partially mimicked and occluded the additional impacts of Iso. This sensitization of TS2-neo CA1 synapses to induction of LTP by PTT stimulation alone could be due to the G406R mutation already enhancing basal LTCC function regardless of S1928 phosphorylation state. Alternatively, the gain-of-function provided by G406R mutation may be allowing additional Ca^{2+} influx through LTCCs in response to PTT stimulation that then engages Ca^{2+}-dependent adenylyl cyclase (AC)-mediated cAMP production and PKA signaling, independent of β-adrenergic receptor-G_s-mediated AC activation. This additional engagement of LTCC-Ca^{2+}-AC-cAMP-PKA signaling in TS2-neo mice could feedback to further enhance LTCC activity via $Ca_V1.2$ S1928 phosphorylation and/or signal downstream to promote AMPAR-GluA1 subunit Ser845 phosphorylation and CP-AMPAR synaptic insertion that is ultimately required for expression of PTT-LTP (Qian et al., 2012; Zhang et al., 2013). Regardless of these mechanisms, the synaptic potentiation in response to PTT stimulation alone in TS2-neo is somehow reducing the additional amount of PTT-LTP able to be produced by β-adrenergic stimulation in that both WT and TS2-neo CA1 synapses ultimately expressed the same maximal amount of potentiation after PTT stimulation in the presence of Iso. The sensitization of LTP to induction by 5 Hz PTT stimulation alone in TS2-neo mice could be relevant for the enhanced contextual fear memory previously observed in TS2-neo mice (Bader et al., 2011). Notably, prior studies have linked sensitization of LTP induction in response to stimulation frequencies in the 5–10 Hz range to enhanced fear learning through pathways involving AMPAR phosphorylation downstream of β-adrenergic receptor signaling (Hu et al., 2007; Qian et al., 2012; Zhang et al., 2013).

4.4. Conclusions

The overall impacts of the $Ca_V1.2$ G406R mutation on both basal transmission and synaptic plasticity that we report here are complex, in some cases unexpected, and not always directly linked to $Ca_V1.2$ gain of function. These impacts could be relevant for altered hippocampal function that underlies ASD-associated cognitive impairments, such as enhanced contextual fear memory, previously characterized in TS2-neo mice (Bader et al., 2011).

Supplementary Material

Refer to Web version on PubMed Central for supplementary material.

Acknowledgements

We thank William Catterall (University of Washington) for generously providing the anti-$Ca_V1.2$-*P*-S1928 antibody. This work was supported by NIH grants R01NS040701 and R01MH123700 to M.L.D., pilot grant funding from the University of Colorado Clinical and Translational Science Institute and Center for Neuroscience to M.L.D. and T.A.B., and the Ponzio Family Chair in Neurology Research (Children's Hospital Colorado Foundation) to T.A.B. The contents are the authors' sole responsibility and do not necessarily represent official NIH views.

Data availability

Data will be made available on request.

References

Bader PL, Faizi M, Kim LH, Owen SF, Tadross MR, Alfa RW, Bett GC, Tsien RW, Rasmusson RL, Shamloo M, 2011. Mouse model of Timothy syndrome recapitulates triad of autistic traits. Proc. Natl. Acad. Sci. U. S. A 108, 15432–15437. [PubMed: 21878566]

Barrett CF, Tsien RW, 2008. The Timothy syndrome mutation differentially affects voltage- and calcium-dependent inactivation of CaV1.2 L-type calcium channels. Proc. Natl. Acad. Sci. U. S. A 105, 2157–2162. [PubMed: 18250309]

Belfield JL, Whittaker C, Cader MZ, Chawla S, 2006. Differential effects of Ca2+ and cAMP on transcription mediated by MEF2D and cAMP-response element-binding protein in hippocampal neurons. J. Biol. Chem 281, 27724–27732. [PubMed: 16870618]

Ben-Ari Y, 2002. Excitatory actions of gaba during development: the nature of the nurture. Nat. Rev. Neurosci 3, 728–739. [PubMed: 12209121]

Ben-Ari Y, 2014. The GABA excitatory/inhibitory developmental sequence: a personal journey. Neuroscience 279, 187–219. [PubMed: 25168736]

Ben-Ari Y, Gaiarsa JL, Tyzio R, Khazipov R, 2007. GABA: a pioneer transmitter that excites immature neurons and generates primitive oscillations. Physiol. Rev 87, 1215–1284. [PubMed: 17928584]

Bernard PB, Castano AM, Bayer KU, Benke TA, 2014. Necessary, but not sufficient: insights into the mechanisms of mGluR mediated long-term depression from a rat model of early life seizures. Neuropharmacology 84, 1–12. [PubMed: 24780380]

Bernard PB, Castano AM, Beitzel CS, Carlson VB, Benke TA, 2015. Behavioral changes following a single episode of early-life seizures support the latent development of an autistic phenotype. Epilepsy Behav. 44, 78–85. [PubMed: 25659043]

Bett GC, Lis A, Wersinger SR, Baizer JS, Duffey ME, Rasmusson RL, 2012. A mouse model of timothy syndrome: a complex autistic disorder resulting from a point mutation in Cav1.2. N. Am. J. Med. Sci 5, 135–140.

Bhat S, Dao DT, Terrillion CE, Arad M, Smith RJ, Soldatov NM, Gould TD, 2012. CACNA1C (Ca(v)1.2) in the pathophysiology of psychiatric disease. Prog. Neurobiol 99 (1), 1–14. 10.1016/j.pneurobio.2012.06.001. [PubMed: 22705413]

Birey F, Li MY, Gordon A, Thete MV, Valencia AM, Revah O, Pasca AM, Geschwind DH, Pasca SP, 2022. Dissecting the molecular basis of human interneuron migration in forebrain assembloids from Timothy syndrome. Cell Stem Cell 29, 248–264 e247. [PubMed: 34990580]

Bozdagi O, Sakurai T, Papapetrou D, Wang X, Dickstein DL, Takahashi N, Kajiwara Y, Yang M, Katz AM, Scattoni ML, Harris MJ, Saxena R, Silverman JL, Crawley JN, Zhou Q, Hof PR, Buxbaum JD, 2010. Haploinsufficiency of the autism-associated Shank3 gene leads to deficits in synaptic function, social interaction, and social communication. Mol. Autism 1, 15. [PubMed: 21167025]

Brooks-Kayal A, 2010. Epilepsy and autism spectrum disorders: are there common developmental mechanisms? Brain Dev. 32, 731–738. [PubMed: 20570072]

Caillard O, Ben-Ari Y, Gaiarsa JL, 1999. Mechanisms of induction and expression of long-term depression at GABAergic synapses in the neonatal rat hippocampus. J. Neurosci 19, 7568–7577. [PubMed: 10460263]

Campiglio M, Coste de Bagneaux P, Ortner NJ, Tuluc P, Van Petegem F, Flucher BE, 2018. STAC proteins associate to the IQ domain of CaV1.2 and inhibit calcium-dependent inactivation. Proc. Natl. Acad. Sci. U. S. A 115, 1376–1381. [PubMed: 29363593]

Catterall WA, 2011. Voltage-gated calcium channels. Cold Spring Harbor Perspect. Biol 3 a003947.

Chao HT, Chen H, Samaco RC, Xue M, Chahrour M, Yoo J, Neul JL, Gong S, Lu HC, Heintz N, Ekker M, Rubenstein JL, Noebels JL, Rosenmund C, Zoghbi HY, 2010. Dysfunction in GABA signalling mediates autism-like stereotypies and Rett syndrome phenotypes. Nature 468, 263–269. [PubMed: 21068835]

Cheng EP, Yuan C, Navedo MF, Dixon RE, Nieves-Cintron M, Scott JD, Santana LF, 2011. Restoration of normal L-type Ca2+ channel function during Timothy syndrome by ablation of an anchoring protein. Circ. Res 109, 255–261. [PubMed: 21700933]

Choong XY, Tosh JL, Pulford LJ, Fisher EM, 2015. Dissecting Alzheimer disease in Down syndrome using mouse models. Front. Behav. Neurosci 9, 268. [PubMed: 26528151]

Collingridge GL, Peineau S, Howland JG, Wang YT, 2010. Long-term depression in the CNS. Nat. Rev. Neurosci 11, 459–473. [PubMed: 20559335]

De Jongh KS, Murphy BJ, Colvin AA, Hell JW, Takahashi M, Catterall WA, 1996. Specific phosphorylation of a site in the full-length form of the alpha 1 subunit of the cardiac L-type calcium channel by adenosine 3',5'-cyclic monophosphate-dependent protein kinase. Biochemistry 35, 10392–10402. [PubMed: 8756695]

Deisseroth K, Bito H, Tsien RW, 1996. Signaling from synapse to nucleus: postsynaptic CREB phosphorylation during multiple forms of hippocampal synaptic plasticity. Neuron 16, 89–101. [PubMed: 8562094]

Di Biase V, Obermair GJ, Szabo Z, Altier C, Sanguesa J, Bourinet E, Flucher BE, 2008. Stable membrane expression of postsynaptic CaV1.2 calcium channel clusters is independent of interactions with AKAP79/150 and PDZ proteins. J. Neurosci 28, 13845–13855. [PubMed: 19091974]

Di Biase V, Tuluc P, Campiglio M, Obermair GJ, Heine M, Flucher BE, 2011. Surface traffic of dendritic CaV1.2 calcium channels in hippocampal neurons. J. Neurosci 31, 13682–13694. [PubMed: 21940459]

Dick IE, Joshi-Mukherjee R, Yang W, Yue DT, 2016. Arrhythmogenesis in Timothy Syndrome is associated with defects in Ca(2+)-dependent inactivation. Nat. Commun 7, 10370. [PubMed: 26822303]

Dittmer PJ, Dell'Acqua ML, Sather WA, 2014. Ca2+/calcineurin-dependent inactivation of neuronal L-type Ca2+ channels requires priming by AKAP-anchored protein kinase A. Cell Rep. 7, 1410–1416. [PubMed: 24835998]

Dittmer PJ, Dell'Acqua ML, Sather WA, 2019. Synaptic crosstalk conferred by a zone of differentially regulated Ca(2+) signaling in the dendritic shaft adjoining a potentiated spine. Proc. Natl. Acad. Sci. U. S. A 116, 13611–13620. [PubMed: 31209051]

Dittmer PJ, Wild AR, Dell'Acqua ML, Sather WA, 2017. STIM1 Ca2+ sensor control of L-type Ca2+-channel-dependent dendritic spine structural plasticity and nuclear signaling. Cell Rep. 19, 321–334. [PubMed: 28402855]

Dixon RE, Yuan C, Cheng EP, Navedo MF, Santana LF, 2012. Ca2+ signaling amplification by oligomerization of L-type Cav1.2 channels. Proc. Natl. Acad. Sci. U. S. A 109, 1749–1754. [PubMed: 22307641]

Dolmetsch R, 2003. Excitation-transcription coupling: signaling by ion channels to the nucleus. Sci. STKE PE4, 2003. [PubMed: 12538881]

Erxleben C, Liao Y, Gentile S, Chin D, Gomez-Alegria C, Mori Y, Birnbaumer L, Armstrong DL, 2006. Cyclosporin and Timothy syndrome increase mode 2 gating of CaV1.2 calcium channels

through aberrant phosphorylation of S6 helices. Proc. Natl. Acad. Sci. U. S. A 103, 3932–3937. [PubMed: 16537462]

Garcia JD, Gookin SE, Crosby KC, Schwartz SL, Tiemeier E, Kennedy MJ, Dell'Acqua ML, Herson PS, Quillinan N, Smith KR, 2021. Stepwise disassembly of GABAergic synapses during pathogenic excitotoxicity. Cell Rep. 37, 110142. [PubMed: 34936876]

Gillberg C, Billstedt E, 2000. Autism and Asperger syndrome: coexistence with other clinical disorders. Acta Psychiatr. Scand 102, 321–330. [PubMed: 11098802]

Gogolla N, Leblanc JJ, Quast KB, Sudhof TC, Fagiolini M, Hensch TK, 2009. Common circuit defect of excitatory-inhibitory balance in mouse models of autism. J. Neurodev. Disord 1, 172–181. [PubMed: 20664807]

Graef IA, Mermelstein PG, Stankunas K, Neilson JR, Deisseroth K, Tsien RW, Crabtree GR, 1999. L-type calcium channels and GSK-3 regulate the activity of NF-ATc4 in hippocampal neurons. Nature 401, 703–708. [PubMed: 10537109]

Greer PL, Greenberg ME, 2008. From synapse to nucleus: calcium-dependent gene transcription in the control of synapse development and function. Neuron 59, 846–860. [PubMed: 18817726]

Grover LM, Teyler TJ, 1990. Two components of long-term potentiation induced by different patterns of afferent activation. Nature 347, 477–479. [PubMed: 1977084]

Guzikowski NJ, Kavalali ET, 2022. Nano-organization of spontaneous GABAergic transmission directs its autonomous function in neuronal signaling. Cell Rep. 40, 111172. [PubMed: 35947950]

Han W, Shepard RD, Lu W, 2021. Regulation of GABAARs by transmembrane accessory proteins. Trends Neurosci. 44, 152–165. [PubMed: 33234346]

Hansen KB, Wollmuth LP, Bowie D, Furukawa H, Menniti FS, Sobolevsky AI, Swanson GT, Swanger SA, Greger IH, Nakagawa T, McBain CJ, Jayaraman V, Low CM, Dell'Acqua ML, Diamond JS, Camp CR, Perszyk RE, Yuan H, Traynelis SF, 2021. Structure, function, and pharmacology of glutamate receptor ion channels. Pharmacol. Rev 73, 298–487. [PubMed: 34753794]

Hiester BG, Bourke AM, Sinnen BL, Cook SG, Gibson ES, Smith KR, Kennedy MJ, 2017. L-type voltage-gated Ca(2+) channels regulate synaptic-activity-triggered recycling endosome fusion in neuronal dendrites. Cell Rep. 21, 2134–2146. [PubMed: 29166605]

Horigane SI, Ozawa Y, Zhang J, Todoroki H, Miao P, Haijima A, Yanagawa Y, Ueda S, Nakamura S, Kakeyama M, Takemoto-Kimura S, 2020. A mouse model of Timothy syndrome exhibits altered social competitive dominance and inhibitory neuron development. FEBS Open Bio 10, 1436–1446.

Hu H, Real E, Takamiya K, Kang MG, Ledoux J, Huganir RL, Malinow R, 2007. Emotion enhances learning via norepinephrine regulation of AMPA-receptor trafficking. Cell 131, 160–173. [PubMed: 17923095]

Huganir RL, Nicoll RA, 2013. AMPARs and synaptic plasticity: the last 25 years. Neuron 80, 704–717. [PubMed: 24183021]

Kamijo S, Ishii Y, Horigane SI, Suzuki K, Ohkura M, Nakai J, Fujii H, Takemoto-Kimura S, Bito H, 2018. A critical neurodevelopmental role for L-type voltage-gated calcium channels in neurite extension and radial migration. J. Neurosci 38, 5551–5566. [PubMed: 29773754]

Kang H, Sun LD, Atkins CM, Soderling TR, Wilson MA, Tonegawa S, 2001. An important role of neural activity-dependent CaMKIV signaling in the consolidation of long-term memory. Cell 106, 771–783. [PubMed: 11572782]

Krey JF, Pasca SP, Shcheglovitov A, Yazawa M, Schwemberger R, Rasmusson R, Dolmetsch RE, 2013. Timothy syndrome is associated with activity-dependent dendritic retraction in rodent and human neurons. Nat. Neurosci 16, 201–209. [PubMed: 23313911]

Langwieser N, Christel CJ, Kleppisch T, Hofmann F, Wotjak CT, Moosmang S, 2010. Homeostatic switch in hebbian plasticity and fear learning after sustained loss of Cav1.2 calcium channels. J. Neurosci 30, 8367–8375. [PubMed: 20573883]

Lewine JD, Andrews R, Chez M, Patil AA, Devinsky O, Smith M, Kanner A, Davis JT, Funke M, Jones G, Chong B, Provencal S, Weisend M, Lee RR, Orrison WW Jr., 1999. Magnetoencephalographic patterns of epileptiform activity in children with regressive autism spectrum disorders. Pediatrics 104, 405–418. [PubMed: 10469763]

Li B, Tadross MR, Tsien RW, 2016. Sequential ionic and conformational signaling by calcium channels drives neuronal gene expression. Science 351, 863–867. [PubMed: 26912895]

Li H, Pink MD, Murphy JG, Stein A, Dell'acqua ML, Hogan PG, 2012. Balanced interactions of calcineurin with AKAP79 regulate Ca(2+)-calcineurin-NFAT signaling. Nat. Struct. Mol. Biol 19, 337–345. [PubMed: 22343722]

Limpitikul WB, Dick IE, Ben-Johny M, Yue DT, 2016. An autism-associated mutation in CaV1.3 channels has opposing effects on voltage- and Ca(2+)-dependent regulation. Sci. Rep 6, 27235. [PubMed: 27255217]

Liu C, Belichenko PV, Zhang L, Fu D, Kleschevnikov AM, Baldini A, Antonarakis SE, Mobley WC, Yu YE, 2011. Mouse models for Down syndrome-associated developmental cognitive disabilities. Dev. Neurosci 33, 404–413. [PubMed: 21865664]

Loomes R, Hull L, Mandy WPL, 2017. What is the male-to-female ratio in autism spectrum disorder? A systematic review and meta-analysis. J. Am. Acad. Child Adolesc. Psychiatry 56, 466–474. [PubMed: 28545751]

Lu AT, Dai X, Martinez-Agosto JA, Cantor RM, 2012. Support for calcium channel gene defects in autism spectrum disorders. Mol. Autism 3, 18. [PubMed: 23241247]

Ma H, Groth RD, Cohen SM, Emery JF, Li B, Hoedt E, Zhang G, Neubert TA, Tsien RW, 2014. gammaCaMKII shuttles Ca(2)(+)/CaM to the nucleus to trigger CREB phosphorylation and gene expression. Cell 159, 281–294. [PubMed: 25303525]

Malenka RC, Bear MF, 2004. LTP and LTD; an embarrassment of riches. Neuron 44, 5–21. [PubMed: 15450156]

McLean HA, Caillard O, Ben-Ari Y, Gaiarsa JL, 1996. Bidirectional plasticity expressed by GABAergic synapses in the neonatal rat hippocampus. J. Physiol 496, 471–477. [PubMed: 8910230]

Mermelstein PG, Bito H, Deisseroth K, Tsien RW, 2000. Critical dependence of cAMP response element-binding protein phosphorylation on L-type calcium channels supports a selective response to EPSPs in preference to action potentials. J. Neurosci 20, 266–273. [PubMed: 10627604]

Moosmang S, Haider N, Klugbauer N, Adelsberger H, Langwieser N, Muller J, Stiess M, Marais E, Schulla V, Lacinova L, Goebbels S, Nave KA, Storm DR, Hofmann F, Kleppisch T, 2005. Role of hippocampal Cav1.2 Ca2+ channels in NMDA receptor-independent synaptic plasticity and spatial memory. J. Neurosci 25, 9883–9892. [PubMed: 16251435]

Murphy JG, Crosby KC, Dittmer PJ, Sather WA, Dell'Acqua ML, 2019. AKAP79/150 recruits the transcription factor NFAT to regulate signaling to the nucleus by neuronal L-type Ca(2+) channels. Mol. Biol. Cell 30, 1743–1756. [PubMed: 31091162]

Murphy JG, Sanderson JL, Gorski JA, Scott JD, Catterall WA, Sather WA, Dell'Acqua ML, 2014. AKAP-anchored PKA maintains neuronal L-type calcium channel activity and NFAT transcriptional signaling. Cell Rep. 7, 1577–1588. [PubMed: 24835999]

Navedo MF, Cheng EP, Yuan C, Votaw S, Molkentin JD, Scott JD, Santana LF, 2010. Increased coupled gating of L-type Ca2+ channels during hypertension and Timothy syndrome. Circ. Res 106, 748–756. [PubMed: 20110531]

Nie F, Wang X, Zhao P, Yang H, Zhu W, Zhao Y, Chen B, Valenzuela RK, Zhang R, Gallitano AL, Ma J, 2015. Genetic analysis of SNPs in CACNA1C and ANK3 gene with schizophrenia: a comprehensive meta-analysis. Am J Med Genet B Neuropsychiatr Genet 168, 637–648. [PubMed: 26227746]

Obermair GJ, Szabo Z, Bourinet E, Flucher BE, 2004. Differential targeting of the L-type Ca2+ channel alpha 1C (CaV1.2) to synaptic and extrasynaptic compartments in hippocampal neurons. Eur. J. Neurosci 19, 2109–2122. [PubMed: 15090038]

Oh WC, Smith KR, 2019. Activity-dependent development of GABAergic synapses. Brain Res. 1707, 18–26. [PubMed: 30439352]

Oliveria SF, Dell'Acqua ML, Sather WA, 2007. AKAP79/150 anchoring of calcineurin controls neuronal L-type Ca2+ channel activity and nuclear signaling. Neuron 55, 261–275. [PubMed: 17640527]

Oliveria SF, Dittmer PJ, Youn DH, Dell'acqua ML, Sather WA, 2012. Localized calcineurin confers Ca2+-dependent inactivation on neuronal L-type Ca2+ channels. J. Neurosci 32, 15328–15337. [PubMed: 23115171]

Park CY, Shcheglovitov A, Dolmetsch R, 2010. The CRAC channel activator STIM1 binds and inhibits L-type voltage-gated calcium channels. Science 330, 101–105. [PubMed: 20929812]

Patriarchi T, Qian H, Di Biase V, Malik ZA, Chowdhury D, Price JL, Hammes EA, Buonarati OR, Westenbroek RE, Catterall WA, Hofmann F, Xiang YK, Murphy GG, Chen CY, Navedo MF, Hell JW, 2016. Phosphorylation of Cav1.2 on S1928 uncouples the L-type Ca2+ channel from the beta2 adrenergic receptor. EMBO J. 35, 1330–1345. [PubMed: 27103070]

Peng YR, Zeng SY, Song HL, Li MY, Yamada MK, Yu X, 2010. Postsynaptic spiking homeostatically induces cell-autonomous regulation of inhibitory inputs via retrograde signaling. J. Neurosci 30, 16220–16231. [PubMed: 21123568]

Pinggera A, Lieb A, Benedetti B, Lampert M, Monteleone S, Liedl KR, Tuluc P, Striessnig J, 2015. CACNA1D de novo mutations in autism spectrum disorders activate Cav1.3 L-type calcium channels. Biol. Psychiatr 77, 816–822.

Pinggera A, Striessnig J, 2016. Cav 1.3 (CACNA1D) L-type Ca(2+) channel dysfunction in CNS disorders. J. Physiol 594, 5839–5849. [PubMed: 26842699]

Pizzarelli R, Cherubini E, 2011. Alterations of GABAergic signaling in autism spectrum disorders. Neural Plast., 297153, 2011. [PubMed: 21766041]

Polster A, Dittmer PJ, Perni S, Bichraoui H, Sather WA, Beam KG, 2018. Stac proteins suppress Ca(2+)-dependent inactivation of neuronal l-type Ca(2+) channels. J. Neurosci 38, 9215–9227. [PubMed: 30201773]

Purkey AM, Dell'Acqua ML, 2020. Phosphorylation-dependent regulation of Ca(2+)-permeable AMPA receptors during hippocampal synaptic plasticity. Front. Synaptic Neurosci 12, 8. [PubMed: 32292336]

Qian H, Matt L, Zhang M, Nguyen M, Patriarchi T, Koval OM, Anderson ME, He K, Lee HK, Hell JW, 2012. beta2-Adrenergic receptor supports prolonged theta tetanus-induced LTP. J. Neurophysiol 107, 2703–2712. [PubMed: 22338020]

Qian H, Patriarchi T, Price JL, Matt L, Lee B, Nieves-Cintron M, Buonarati OR, Chowdhury D, Nanou E, Nystoriak MA, Catterall WA, Poomvanicha M, Hofmann F, Navedo MF, Hell JW, 2017. Phosphorylation of Ser1928 mediates the enhanced activity of the L-type Ca2+ channel Cav1.2 by the beta2-adrenergic receptor in neurons. Sci. Signal 10.

Quadrato G, Elnaggar MY, Duman C, Sabino A, Forsberg K, Di Giovanni S, 2014. Modulation of GABAA receptor signaling increases neurogenesis and suppresses anxiety through NFATc4. J. Neurosci 34, 8630–8645. [PubMed: 24948817]

Rajgor D, Purkey AM, Sanderson JL, Welle TM, Garcia JD, Dell'Acqua ML, Smith KR, 2020. Local miRNA-dependent translational control of GABAAR synthesis during inhibitory long-term potentiation. Cell Rep. 31, 107785. [PubMed: 32579917]

Sanderson JL, Freund RK, Gorski JA, Dell'Acqua ML, 2021. beta-Amyloid disruption of LTP/LTD balance is mediated by AKAP150-anchored PKA and Calcineurin regulation of Ca(2+)-permeable AMPA receptors. Cell Rep. 37, 109786. [PubMed: 34610314]

Sanderson JL, Gorski JA, Dell'Acqua ML, 2016. NMDA receptor-dependent LTD requires transient synaptic incorporation of Ca(2+)-permeable AMPARs mediated by AKAP150-anchored PKA and calcineurin. Neuron 89, 1000–1015. [PubMed: 26938443]

Sanderson JL, Gorski JA, Gibson ES, Lam P, Freund RK, Chick WS, Dell'Acqua ML, 2012. AKAP150-anchored calcineurin regulates synaptic plasticity by limiting synaptic incorporation of Ca2+-permeable AMPA receptors. J. Neurosci 32, 15036–15052. [PubMed: 23100425]

Servili E, Trus M, Sajman J, Sherman E, Atlas D, 2020. Elevated basal transcription can underlie timothy channel association with autism related disorders. Prog. Neurobiol 191, 101820. [PubMed: 32437834]

Silverman JL, Yang M, Lord C, Crawley JN, 2010. Behavioural phenotyping assays for mouse models of autism. Nat. Rev. Neurosci 11, 490–502. [PubMed: 20559336]

Singh B, Henneberger C, Betances D, Arevalo MA, Rodriguez-Tebar A, Meier JC, Grantyn R, 2006. Altered balance of glutamatergic/GABAergic synaptic input and associated changes in dendrite

morphology after BDNF expression in BDNF-deficient hippocampal neurons. J. Neurosci 26, 7189–7200. [PubMed: 16822976]

Smith KR, Kittler JT, 2010. The cell biology of synaptic inhibition in health and disease. Curr. Opin. Neurobiol 20, 550–556. [PubMed: 20650630]

Smoller JW, Craddock N, Kendler K, Lee PH, Neale BM, Nurnberger JI, Ripke S, Santangelo S, Sullivan PF, 2013. Identification of risk loci with shared effects on five major psychiatric disorders: a genome-wide analysis. Lancet 381, 1371–1379. [PubMed: 23453885]

Splawski I, Timothy KW, Sharpe LM, Decher N, Kumar P, Bloise R, Napolitano C, Schwartz PJ, Joseph RM, Condouris K, Tager-Flusberg H, Priori SG, Sanguinetti MC, Keating MT, 2004. Ca(V)1.2 calcium channel dysfunction causes a multisystem disorder including arrhythmia and autism. Cell 119, 19–31. [PubMed: 15454078]

Tabuchi K, Blundell J, Etherton MR, Hammer RE, Liu X, Powell CM, Sudhof TC, 2007. A neuroligin-3 mutation implicated in autism increases inhibitory synaptic transmission in mice. Science 318, 71–76. [PubMed: 17823315]

Turrigiano G, 2012. Homeostatic synaptic plasticity: local and global mechanisms for stabilizing neuronal function. Cold Spring Harbor Perspect. Biol 4, a005736.

Wang Y, Deng X, Mancarella S, Hendron E, Eguchi S, Soboloff J, Tang XD, Gill DL, 2010. The calcium store sensor, STIM1, reciprocally controls Orai and CaV1.2 channels. Science 330, 105–109. [PubMed: 20929813]

Wheeler DG, Barrett CF, Groth RD, Safa P, Tsien RW, 2008. CaMKII locally encodes L-type channel activity to signal to nuclear CREB in excitation-transcription coupling. J. Cell Biol 183, 849–863. [PubMed: 19047462]

Wheeler DG, Groth RD, Ma H, Barrett CF, Owen SF, Safa P, Tsien RW, 2012. Ca(V)1 and Ca(V)2 channels engage distinct modes of Ca(2+) signaling to control CREB-dependent gene expression. Cell 149, 1112–1124. [PubMed: 22632974]

Wheless JW, Simos PG, Butler IJ, 2002. Language dysfunction in epileptic conditions. Semin. Pediatr. Neurol 9, 218–228. [PubMed: 12350043]

Wild AR, Sinnen BL, Dittmer PJ, Kennedy MJ, Sather WA, Dell'Acqua ML, 2019. Synapse-to-Nucleus communication through NFAT is mediated by L-type Ca(2 +) channel Ca(2+) spike propagation to the soma. Cell Rep. 26, 3537–3550 e3534. [PubMed: 30917310]

Wu GY, Deisseroth K, Tsien RW, 2001. Activity-dependent CREB phosphorylation: convergence of a fast, sensitive calmodulin kinase pathway and a slow, less sensitive mitogen-activated protein kinase pathway. Proc. Natl. Acad. Sci. U. S. A 98, 2808–2813. [PubMed: 11226322]

Yazawa M, Hsueh B, Jia X, Pasca AM, Bernstein JA, Hallmayer J, Dolmetsch RE, 2011. Using induced pluripotent stem cells to investigate cardiac phenotypes in Timothy syndrome. Nature 471, 230–234. [PubMed: 21307850]

Zhang C, Atasoy D, Arac D, Yang X, Fucillo MV, Robison AJ, Ko J, Brunger AT, Sudhof TC, 2010. Neurexins physically and functionally interact with GABA(A) receptors. Neuron 66, 403–416. [PubMed: 20471353]

Zhang M, Patriarchi T, Stein IS, Qian H, Matt L, Nguyen M, Xiang YK, Hell JW, 2013. Adenylyl cyclase anchoring by a kinase anchor protein AKAP5 (AKAP79/ 150) is important for postsynaptic beta-adrenergic signaling. J. Biol. Chem 288, 17918–17931. [PubMed: 23649627]

Zhou Y, Kaiser T, Monteiro P, Zhang X, Van der Goes MS, Wang D, Barak B, Zeng M, Li C, Lu C, Wells M, Amaya A, Nguyen S, Lewis M, Sanjana N, Zhang M, Zhang F, Fu Z, Feng G, 2016. Mice with Shank3 mutations associated with ASD and schizophrenia display both shared and distinct defects. Neuron 89, 147–162. [PubMed: 26687841]

Zucca S, Valenzuela CF, 2010. Low concentrations of alcohol inhibit BDNF-dependent GABAergic plasticity via L-type Ca2+ channel inhibition in developing CA3 hippocampal pyramidal neurons. J. Neurosci 30, 6776–6781. [PubMed: 20463239]

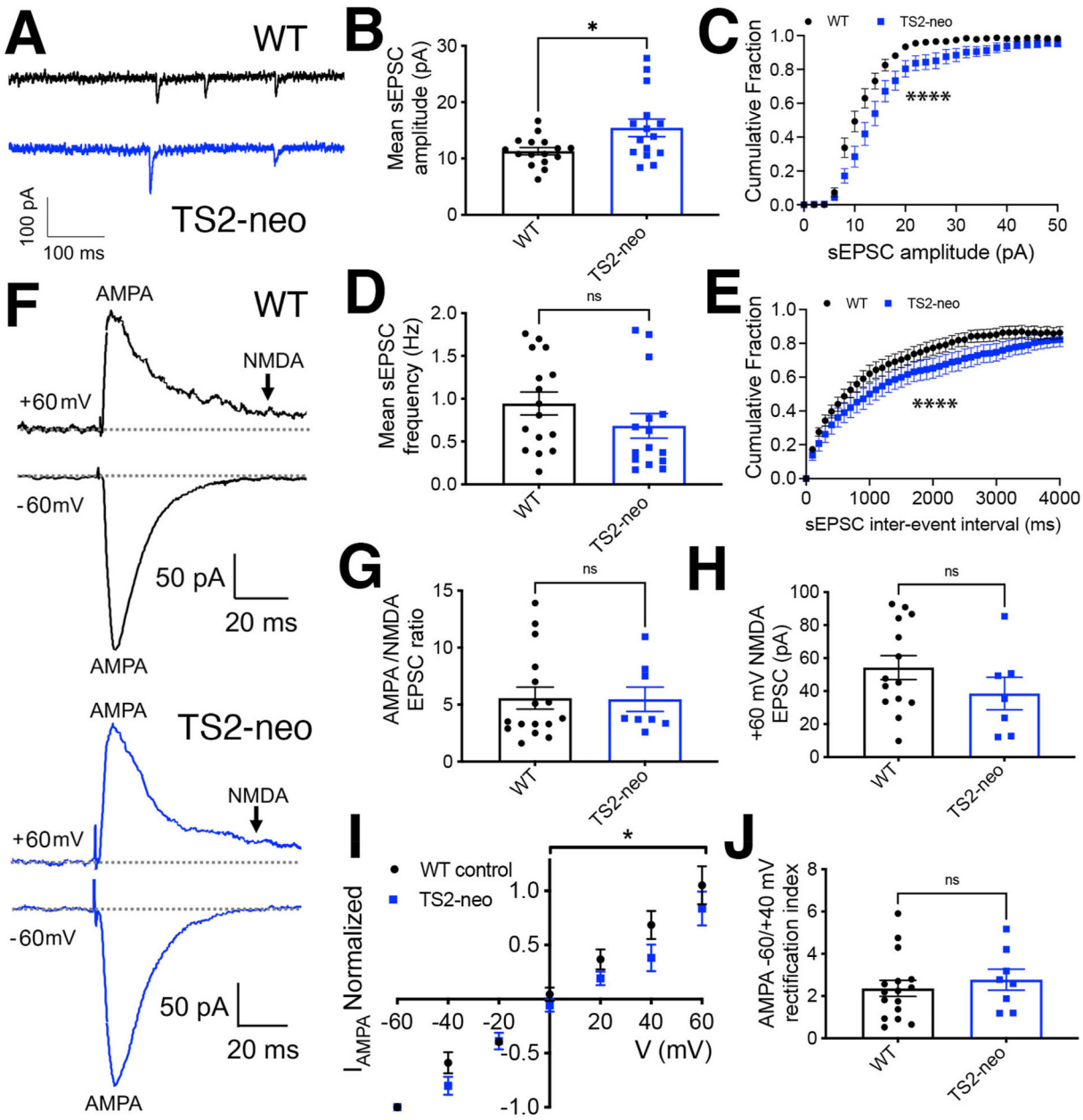

Fig. 1. Increased basal excitatory synaptic input to CA1 neurons in TS2-neo mice.

(A) Representative recordings of AMPAR-mediated sEPSC responses from CA1 neurons in acute hippocampal slices from WT and TS2-neo mice. (B) Plots of mean sEPSC amplitude (*p < 0.05 by *t*-test) and (C) cumulative distributions of sEPSC amplitudes for WT and TS2-neo mice (*p < 0.05 by K–S test). (D) Plot of mean sEPSC frequency (p > 0.05, ns by *t*-test) and (E) cumulative distributions of sEPSC interevent intervals for WT and TS2-neo mice (****p < 0.0001 by K–S test). (F) Representative recordings of evoked inward −60 mV AMPA and outward +60 mV AMPA plus NMDA SC-CA1 EPSC responses for WT and TS2-neo mice. (G) Plots of mean evoked SC-CA1 AMPA/NMDA EPSC amplitude ratios and (H) NMDA EPSC amplitudes in acute hippocampal slices from WT and TS2-neo mice (p > 0.05, ns by *t*-test). (I) I–V plot of evoked AMPA EPSC amplitude (normalized

to EPSC amplitude recorded at −60 mV) versus membrane holding potential (*$p < 0.05$ by two-way ANOVA) and (J) mean AMPA −60/+40 mV EPSC rectification indices (RI) in acute hippocampal slices from WT and TS2-neo mice ($p > 0.05$, ns by *t*-test).

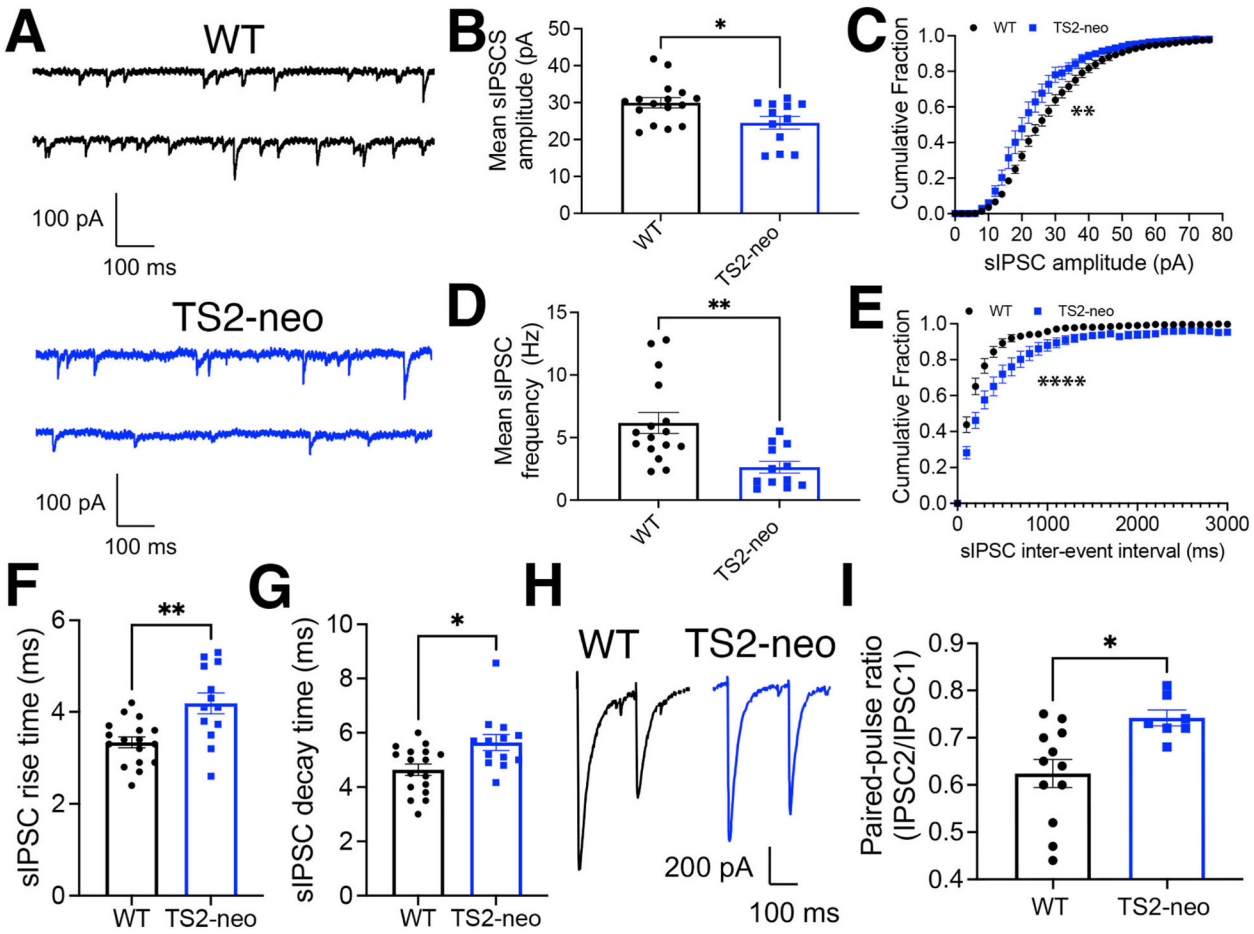

Fig. 2. Decreased basal inhibitory synaptic input to CA1 neurons in TS2-neo mice.

(A) Representative recordings of $GABA_AR$-mediated sIPSC responses from CA1 neurons in acute hippocampal slices from WT and TS2-neo mice. (B) Plots of mean sIPSC amplitude (*p < 0.05 by *t*-test) and (C) cumulative distributions of sIPSC amplitudes for WT and TS2-neo mice (**p < 0.01 by K–S test). (D) Plot of mean sIPSC frequency (**p < 0.01 by *t*-test) and (E) cumulative distributions of sIPSC interevent intervals for WT and TS2-neo mice (****p < 0.0001 by K–S test). (F) Plots of sIPSC rise time (**p < 0.01 by *t*-test) and (G) decay time (*p < 0.05 by Mann-Whitney test) for WT and TS2-neo mice. (H) Representative recordings evoked CA1 IPSCs to measure GABA PPR in acute hippocampal slices from WT and TS2-neo mice. (I) Plot of mean GABA PPR for WT and TS2-neo mice (*p < 0.05 by *t*-test).

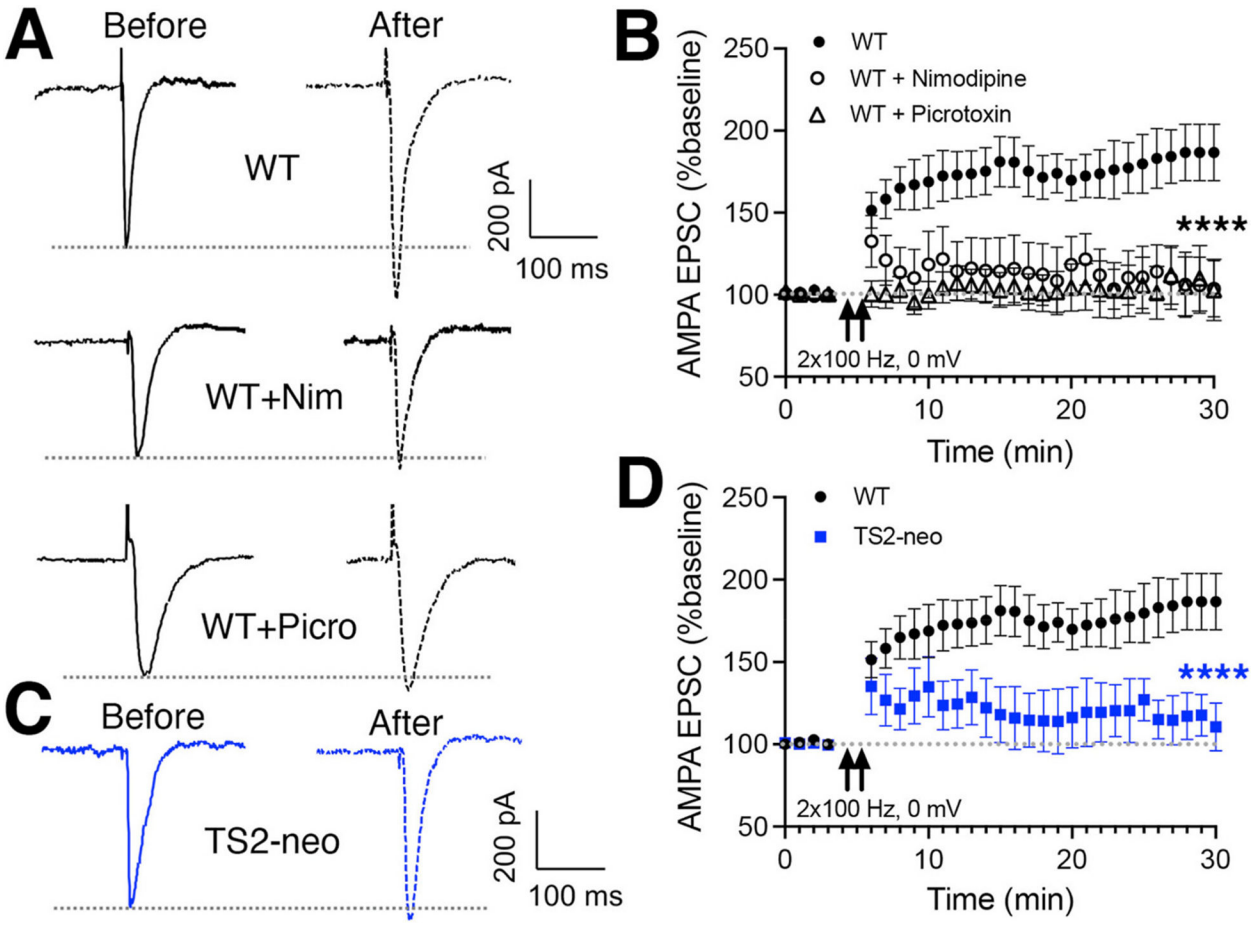

Fig. 3. Impaired LTCC-dependent HFS-LTP at SC-CA1 synapses in TS2-neo mice.

(A) Representative recordings evoked SC-CA1 AMPA EPSC responses (at ~ −40 mV) before and after induction of LTP in WT hippocampal slices by 2 × 100 Hz HFS (1s trains delivered 20 s apart, paired with depolarization to 0 mV, in the presence of MK801 and D-APV) under control conditions and in the presence of either the LTCC antagonist nimodipine (10 μM) or the $GABA_AR$ antagonist picrotoxin (50 μM). (B) Time plots of mean AMPA EPSC responses (normalized to baseline) before and after induction of 2 × 100 Hz HFS LTP under control conditions and in the presence of either the LTCC antagonist nimodipine (****$p < 0.0001$ by two-way ANOVA compared to WT control for last 5 min) or the $GABA_AR$ antagonist picrotoxin (****$p < 0.0001$ by two-way ANOVA compared to WT control for last 5 min). (C) Representative recordings of evoked SC-CA1 AMPA EPSC responses (at ~ −40 mV) before and after induction of 2 × 100 Hz HFS LTP in TS2-neo hippocampal slices. (D) Time plots of mean AMPA EPSC responses (normalized to baseline) before and after induction of 2 × 100 Hz HFS LTP in TS2-neo compared to WT hippocampal slices (****$p < 0.0001$ by two-way ANOVA compared to WT for last 5 min).

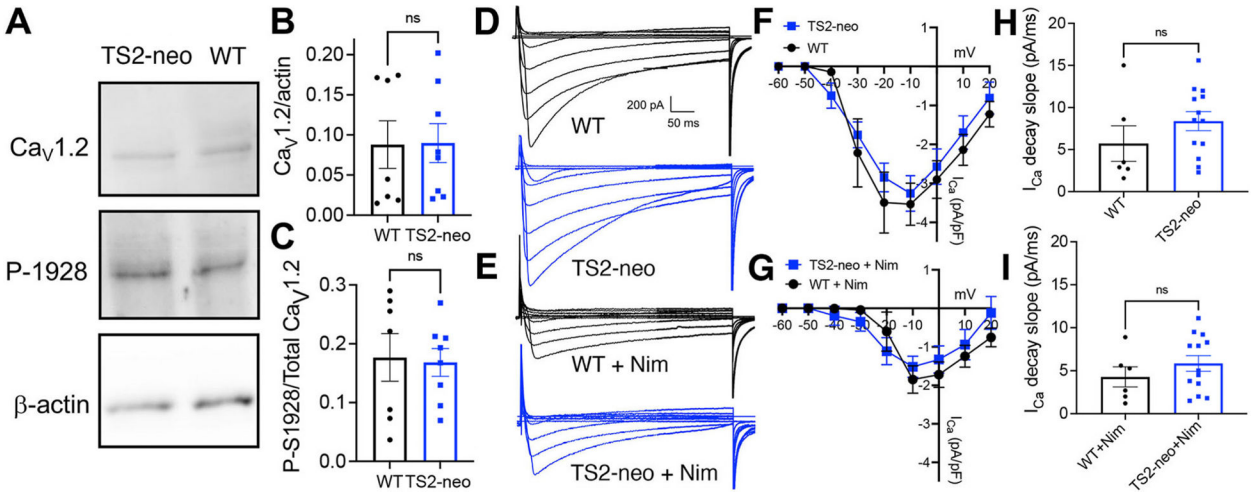

Fig. 4. Normal $Ca_V1.2$ expression, basal S1928 phosphorylation levels, and LTCC Ca^{2+} current density in CA1 neurons from TS2-neo mice.

(A). Representative immunoblots for $Ca_V1.2$ total expression, phospho-S1928, and β-actin (loading control) for whole homogenates of hippocampal slices from WT and TS2-neo mice (see Supplemental Fig. 2 for raw immunoblot images). (B) Quantification of total $Ca_V1.2$ expression levels (normalized to β-actin; $p > 0.05$, ns by *t*-test) and (C) $Ca_V1.2$ S1928 phosphorylation levels (normalized to total $Ca_V1.2$ expression; $p > 0.05$, ns by *t*-test) in whole homogenates of hippocampal slices from WT and TS2-neo mice. (D,E) Representative recordings and (F,G) I_{Ca} density versus voltage (I–V) plots in CA1 neurons from WT and TS2-neo mice in response to 500 ms step depolarization to a range f membrane holding potentials under control conditions (D,F; $p > 0.05$, ns by two-way ANOVA) and following the addition of the LTCC antagonist nimodipine (10 μM)(E,G; $p > 0.05$, ns by two-way ANOVA). (H,I) Decay slope measurements for I_{Ca} measured in response to 500 ms step depolarization to −10 mV for WT and TS2-neo mice under control conditions (H; $p > 0.05$, ns by Mann-Whitney test) and following the addition of nimodipine (I; $p > 0.05$, ns by Mann-Whitney test).

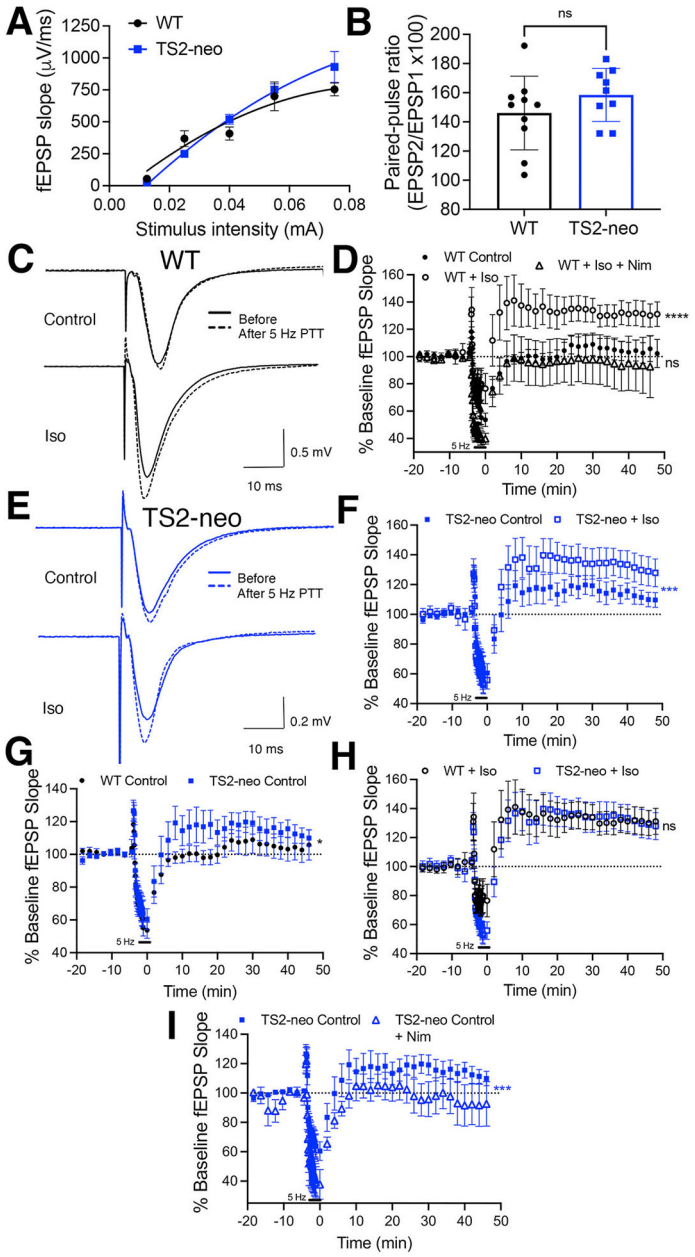

Fig. 5. Sensitization of CA1 synapses in TS2-neo mice to 5 Hz PTT stimulation partially mimics and occludes induction of β-adrenergic receptor-dependent PTT-LTP.

(A) I–O curves plotting fEPSP slope as a function of stimulus intensity for SC-CA1 synapses in WT and Ts2-neo mice ($p > 0.05$, ns by two-way ANOVA). (B) Measurements of paired-pulse fEPSP ratios (PPR with 50 ms inter-stimulus interval) for SC-CA1 synapses in WT and TS2-neo mice ($p > 0.05$, ns by *t*-test). (C) Representative SC-CA1 fEPSP recordings and (D) time plots of fEPSP slope (normalized to baseline) before and after 5Hz PTT stimulation alone or with addition of the β-adrenergic receptor agonist isoproterenol (Iso, 3 μM) and also with the addition of nimodipine (Nim, 10 μM) for hippocampal slices from WT mice (****$p < 0.0001$ by two-way ANOVA for the last 10 min compared to control and Iso + Nim; $p > 0.05$, ns by two-way ANOVA compared to control). (E)

Representative SC-CA1 fEPSP recordings and (F) time plots of fEPSP slope (normalized to baseline) before and after 5Hz PTT stimulation alone or with addition of Iso for hippocampal slices form TS2-neo mice (***$p < 0.001$ by two-way ANOVA for the last 10 min). (G) Time plots of fEPSP slope before and after 5Hz PTT stimulation in slices from WT and TS2-neo mice (*$p < 0.05$ by two-way ANOVA for the last 10 min). (H) Time plots of fEPSP slope before and after 5Hz PTT stimulation with the addition of Iso in slices from WT and TS2-neo mice ($p > 0.05$, ns by two-way ANOVA for the last 10 min). (I) Time plots of fEPSP slope before and after 5Hz PTT stimulation alone in slices from TS2-neo mice under control conditions or with the addition of nimodipine (Nim, 10 μM)(***$p < 0.001$ by two-way ANOVA for the last 10 min).